# Effects of intruder states in $^{179}$Ir

H.-Q. Jin,* L. L. Riedinger, C. R. Bingham, M. P. Carpenter,† V. P. Janzen,‡ C.-H. Yu,* and L. Zhou
*Physics Department, University of Tennessee, Knoxville, Tennessee 37996*

P. B. Semmes,§ J.-Y. Zhang, and M. A. Riley‖
*Joint Institute for Heavy Ion Research, ORNL, Oak Ridge, Tennessee 37831*

C. Baktash, M. L. Halbert, N. R. Johnson, I. Y. Lee,¶ and F. K. McGowan
*Oak Ridge National Laboratory, Oak Ridge, Tennessee 37831*
(Received 20 December 1995)

High-spin states of the odd-$A$ $^{179}$Ir have been studied via heavy-ion fusion reaction. Bands built on five different Nilsson states ($\pi h_{9/2}$, $\pi i_{13/2}$, $\pi d_{5/2}$, $\pi h_{11/2}$, and $\pi f_{7/2}$) have been established, among which the $\pi f_{7/2}$ ($1/2^-[530]$) band is identified for the first time in Ir isotopes. Experimental aligned angular momenta, band-crossing frequencies, and relative transition rates are analyzed and compared with the cranked shell model and the particle-rotor model calculations. Effects of intruder states, particularly $\pi h_{9/2}$ and $\pi i_{13/2}$, have been discussed on three aspects: deformation driving, shape evolution, and quasiparticle alignment. It is found that the $\pi i_{13/2}$ orbital has a strong, positive-$\beta_2$ driving effect on the shape of Ir nuclei, while the driving force of the $\pi h_{9/2}$ orbital is minimized when the Fermi level reaches the shell. The total Routhian surface calculations suggest that the $\pi h_{11/2}$ and $\pi d_{5/2}$ configurations in $^{179}$Ir possess relatively large $\beta_2$ deformation ($\sim$0.26), which is consistent with the particle-rotor calculations. The possible contribution of the $\pi h_{9/2}$ crossing to the gradual alignment gains observed in the $\pi h_{11/2}$ and $\pi d_{5/2}$ bands is discussed from the influence of deformation and interaction strength. [S0556-2813(96)00805-9]

PACS number(s): 23.20.Lv, −21.10.Re, −21.10.Tg, −27.70.+q

## I. INTRODUCTION

It is well known that high-$j$ low-$\Omega$ orbitals play a very important role in determining the underlying properties of nuclear structure. In the rare-earth region, the 1/2[541] (from $\pi h_{9/2}$) and 1/2[660] (from $\pi i_{13/2}$) Nilsson states are commonly referred to as intruder[1] orbitals, since they emanate from above the $Z=82$ gap, rapidly lower in energy with increasing quadrupole $\beta_2$ deformation, and *intrude* into the lower oscillator shell. The occupation of these orbitals by a single proton is expected to have substantial effects on the nuclear shape. Analogously, it has been reported [1] that the neutron $i_{13/2}$ intruder in the $A=130$ region demonstrates large deformation driving effects. It is also commonly known that the first band crossing occurring throughout the rare-earth region is due to the alignment of a $\nu i_{13/2}$ pair resulting from a strong Coriolis interaction. In the heavier Ir-Pt-Au region the alignable $h_{9/2}$ proton pair is gradually coming into play at low rotational frequencies.

In recent years, studies on the lighter Re and Ir nuclei have shown many interesting configuration dependent high-spin phenomena, where bands built on the $\pi d_{5/2}$, $\pi h_{9/2}$, $\pi h_{11/2}$, and $\pi i_{13/2}$ states have been observed. One of the more striking features is the very different pattern of the aligned angular momentum as a function of rotational frequency for the observed bands. The available data in odd-$A$ Re and Ir isotopes ($^{171-175}$Re [2–4] and $^{173-177}$Ir [5–7]), and our new high-spin data in $^{179}$Ir presented here illustrate a $\pi i_{13/2}$ band with steadily increasing alignment in the observed frequency range (typically $0.1<\hbar\omega<0.38$ MeV) when referred to the $\pi h_{9/2}$ band. However, in $^{177}$Re [8,9] and in $^{181}$Ir [10,11] there are sets of positive parity bands that contain the $\pi i_{13/2}$ excitation but also other mixed configurations. Gradual increases in aligned angular momentum have also been observed in the $\pi h_{11/2}$ and $\pi d_{5/2}$ bands. In the same frequency range, a sharp backbending is present in the $\pi h_{9/2}$ band at $\hbar\omega\approx 0.3$ MeV.

The gradual increase of alignment in the $\pi i_{13/2}$, $\pi h_{11/2}$, and $\pi d_{5/2}$ bands is very interesting and in need of a full explanation. One suggestion attributes this feature to a band crossing with a very large interaction, but it is difficult to explain the low-frequency occurrence of the band crossing in a configuration ($\pi i_{13/2}$) that is so strongly deformation driving. An alternative interpretation attributes this gradual alignment gain to a ''$d$ band,'' formed from a pair of $\pi h_{9/2}$ coupled to spin $J=0$, crossing with the ground band at higher rotational frequencies. This has been suggested [6,11–14] to explain the anomalous alignments in the yrast

*Present address: Oak Ridge National Laboratory, Oak Ridge, TN 37831.

†Present address: Argonne National Laboratory, Physics Division, 9700 Cass Avenue, Argonne, IL 60439.

‡Present address: Chalk River Nuclear Laboratories, Atomic Energy of Canada Ltd., Chalk River, Ontario, Canada K0J 1J0.

§Permanent address: Tennessee Technological University, Cookeville, TN 38505.

‖Present address: Department of Physics, Florida State University, Tallahassee, FL 32306.

¶Present address: Lawrence Berkeley National Laboratory, Berkeley, CA 94720.

[1]The conventional meaning of ''intruder'' is slightly modified here. It normally refers to the unique or abnormal parity state.

 

bands of Os and bands ($\pi h_{11/2}$ and $\pi d_{5/2}$) of Re and Ir nuclei. The third suggestion could be that the smooth increase could result from the inappropriate reference in the alignment plot, due to a substantially larger deformation ($\beta_2$) compared with other bands. The peculiar alignment behavior of the $\pi d_{5/2}$ band in $^{183}$Ir was explained by Janzen *et al.* [15] as a $\nu i_{13/2}$ crossing plus a $\pi h_{9/2}$ crossing. The evidence of the $\pi h_{9/2}$ crossing was reported from the studies of double-blocking experiments in odd-odd nuclei by Kreiner *et al.* [16] and Janzen *et al.* [17].

To address these issues, we have performed spectroscopic experiments and also a lifetime measurement on high-spin states in $^{179}$Ir (Secs. II and III), and have made systematic analyses of band crossings and shape changes for bands built on different orbitals in this region (Sec. IV). These studies have been aimed at understanding better the effects of intruder states from three aspects: deformation driving, shape evolution, and quasiparticle alignment. In addition, we have compared the experimental results with calculations using a particle-rotor model for electromagnetic properties, the total Routhian surface for nuclear shapes, and cranked shell model for band crossings.

## II. EXPERIMENTAL INFORMATION

The $\gamma$-ray spectroscopic studies of $^{179}$Ir were carried out at the Oak Ridge National Laboratory. A $^{27}$Al beam was delivered from the tandem accelerator at the Holifield Heavy-Ion Research Facility. The experiment was performed on the spin spectrometer, consisting of 19 Compton-suppressed Ge counters[2] and 52 NaI detectors. The NaI detectors were used as an $H$–$K$ filter, allowing a gate on the $\gamma$-ray total energy and fold of each event to do channel selection. The contributions from the Ge detectors and the anti-Compton shields were taken into account for calculating the values of $H$ and $K$. Stacked x-ray absorbers of Sn, Cu, and Ta were placed in front of mostly the forward-angle Ge detectors to reduce the singles rates in the detectors. A thick lead collimator was added to the inner surface of each Compton shield to prevent target $\gamma$ rays from directly entering the shield.

Levels in $^{179}$Ir were populated by the $^{156}$Gd($^{27}$Al, $4n$) reaction. A Gd target with thickness of 1 mg/cm$^2$ and a $^{208}$Pb backing ($\sim$13 mg/cm$^2$) was used to avoid Doppler shifting in the $\gamma$-ray energies at different detecting angles. The use of a backed target also enabled the extraction of lifetimes of some transitions by the Doppler shift attenuation method (DSAM). Priori to the main experiment, excitation function was measured at three energies of 134, 139, and 144 MeV in order to select the optimal beam energy for the reaction channel of interest. A full measurement was performed at the beam energy of 134 MeV.

Data were recorded in an event-by-event mode, requiring the simultaneous firing of at least two Ge and four NaI detectors. The $\gamma$-$\gamma$ coincidence data were sorted off line into a $4k\times4k$ matrix so that the level scheme could be established from the coincidence relationship. The total detected energy $H$ and fold $K$ were properly gated (''banana'' gate) during the creation of the $\gamma$-$\gamma$ matrix to select mostly the $4n$ channel. With the $H$–$K$ selection, about $80\times10^6$ $\gamma$-$\gamma$ coincidence data were collected in the $^{179}$Ir matrix. A full background subtraction based on the method of Palameta-Waddington [18] was performed on the matrix.

A method based on the observation of directional correlations of $\gamma$ rays deexciting oriented states (DCO ratios) was adopted to determine the $\gamma$-ray multipolarities and spins of the nuclear levels. For this purpose, a $1k\times1k$ DCO matrix was created by sorting data with Ge counters at angle of 24° on one axis compared to those at 63° on the other, and the experimental DCO ratio is calculated by

$$R_{\mathrm{DCO}}=\frac{I_{\gamma_2}^{\theta_1}(\mathrm{gate}_{\gamma_1}^{\theta_2})}{I_{\gamma_2}^{\theta_2}(\mathrm{gate}_{\gamma_1}^{\theta_1})},$$

where $I_{\gamma_2}^{\theta_1}(\mathrm{gate}_{\gamma_1}^{\theta_2})$ is the intensity of $\gamma_2$ on angle $\theta_1$ with the energy gate of $\gamma_1$ on angle $\theta_2$. Usually the gate is chosen to set on a stretched quadrupole ($E2$) transition, then theoretically $R_{\mathrm{DCO}}=1.0$ is expected for stretched $E2$ transitions and $\sim$0.6 for $\Delta I=1$ transitions.

The Ge detectors in the spin spectrometer can be grouped into five rings with angles relative to the beam axis at $\theta=24°$, 63°, 87°, 117°, and 156°. To facilitate the lifetime analysis in $^{179}$Ir, we sorted the events into five $2k\times2k$ matrices, containing the coincidences of $\gamma$ rays between the Ge detectors at one of the rings on one axis and any other correlated Ge on the other axis. Line shapes were measured from spectra gated on transitions lying below the levels for which lifetimes are to be obtained.

## III. EXPERIMENTAL RESULTS

This section is devoted to the discussion of the deduced level scheme and band assignments in $^{179}$Ir. An interesting topic of interband transitions in $^{179}$Ir will be discussed in Sec. III C. The DSAM lifetime measurement is described in Sec. III D.

### A. The level scheme of $^{179}$Ir

From the analysis of the $\gamma$-$\gamma$ matrix, intensities of transitions, DCO ratios, and $H$–$K$ distributions, we have established the level scheme of $^{179}$Ir, as shown in Fig. 1. Nine decay sequences have been identified, labeled from band 1 to band 7, among which bands 3 and 4 consist of two strongly coupled sequences. The $\gamma$ rays identified with this nucleus are summarized in Table I according to their energies, relative intensities, DCO ratios, spin and multipolarity assignments. The relative intensities of $\gamma$ rays were mostly obtained from fitting the total projection spectrum. For those contaminated peaks (doublets, triplets), the gated spectra were used and the results were then normalized to those from the total projection.

The ground state of $^{179}$Ir has been identified [19] to be $5/2^-$ from decay studies. This is the bandhead of the $1/2^-[541]\pi h_{9/2}$ sequence. Due to the large decoupling parameter of this configuration, usually the $9/2^-$ and $5/2^-$ states are separated only by several tens of keV and the di-

[2]During the experiment, two Ge counters were malfunctioning and data from only 17 Ge detectors were used.

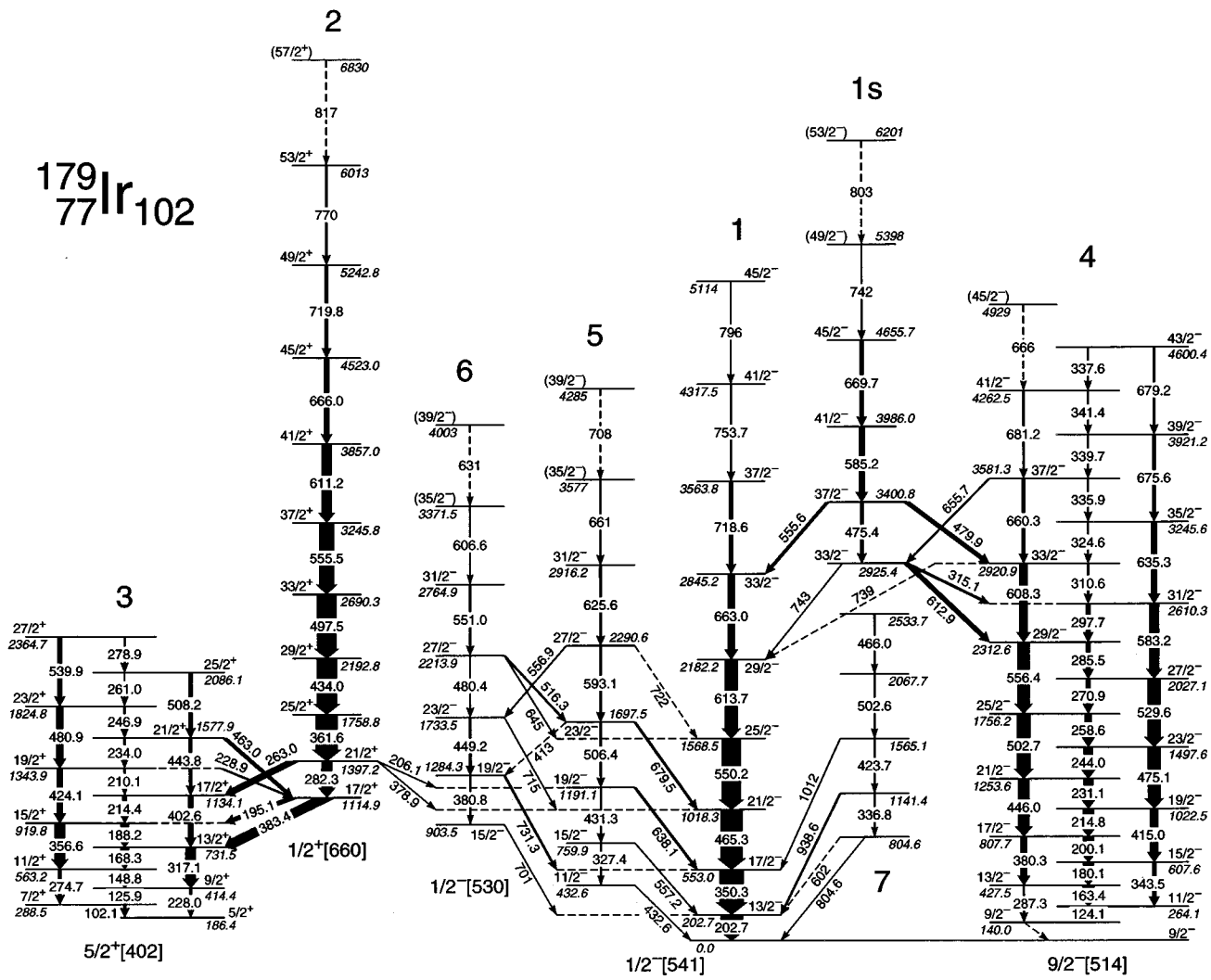


FIG. 1. Level scheme of $^{179}$Ir. The arrow width is proportional to the intensity of the corresponding transition. Transitions to the expected $5/2^-$ ground state are not observed in the experiment and the $9/2^-$ state is used as a reference for the whole level scheme.

rect $\gamma$ transition between these two levels is rarely seen. The $5/2^-$ level is not seen in our data, therefore, the $9/2^-$ state is the lowest level in the current level scheme and the energy of this level has been set to 0 keV as a reference for the entire level scheme.

The spin and parity assignments rely on the DCO ratios as well as the knowledge of band structures (Nilsson configurations) and the systematic information of neighboring nuclei, which will be discussed in the following subsections. The Nilsson configurations associated with bands in $^{179}$Ir presumably are $1/2^-[541]$, $\pi h_{9/2}$ (bands 1 and 5); $1/2^+[660]$, $\pi i_{13/2}$ (band 2); $5/2^+[402]$, $\pi d_{5/2}$ (band 3); $9/2^-[514]$, $\pi h_{11/2}$ (band 4); and $1/2^-[530]$, $\pi f_{7/2}$ (band 6). These assignments are also supported by the analysis of $B(M1)/B(E2)$ branching ratios (see Sec. IV E 1).

A preliminary report of our results was given earlier (Ref. [20]). The $B(M1)/B(E2)$ magnetic and electric quadrupole properties of the $h_{11/2}$ band in $^{179}$Ir were discussed by Dracoulis *et al.* [12]. Lifetime measurements on some of the low-lying states in $^{179}$Ir using the recoil distance method were reported by Müller *et al.* [21] and will be compared with our DSAM results.

### *1. Bands 1 and 1s*

Band 1 is the strongest sequence populated in the reaction, which can be seen from the intensities of $\gamma$ rays listed in Table I. A typical rotational spectrum is illustrated in Fig. 2(a) from the 663.0-keV gate. The DCO ratios of transitions in the band are mostly around 1.0 and are in agreement with the $E2$ assignments.

One of the important measurables used to determine the band configuration is the energy splitting between the two signatures of the band (signature splitting). Band 1 has decoupled characteristics, which implies a low-$K$ structure at their bandheads. The favored-signature sequence is strongly populated in experiment, while the unfavored-signature sequence lies higher in energy and is only weakly populated. Figure 3 shows the calculated single-proton levels around $Z=77$ using the Woods-Saxon potential with $\gamma=0°$ and $\beta_4=0$. There are four Nilsson orbitals of low $K$ on the prolate-deformed side ($\beta_2\sim0.25$) close to the $Z=77$ Fermi surface: $1/2^-[541]$ and $3/2^-[532]$ from the $\pi h_{9/2}$ subshell, $1/2^+[660]$ ($\pi i_{13/2}$), and $1/2^-[530]$ ($\pi f_{7/2}$).

The $1/2^-[541]$ state from the $\pi h_{9/2}$ subshell has been identified as the ground configuration of light odd-$A$ Au and

TABLE I. $\gamma$-ray energies, relative intensities, DCO ratios, and multipolarity assignments in $^{179}$Ir.

| $E_\gamma$ (keV) [a] | Band | $I_\gamma$ [b] | $R_{DCO}$ [c] | $J_i^\pi \rightarrow J_f^\pi$ | Multipolarity |
|---|---|---|---|---|---|
| 202.7 | 1 | 95.2 ± 0.9 | 0.86 ± 0.02 | $13/2^- \rightarrow 9/2^-$ | $E2$ |
| 350.3 | 1 | 100.0 ± 1.0 | 1.08 ± 0.03 | $17/2^- \rightarrow 13/2^-$ | $E2$ |
| 465.3 | 1 | 91.7 ± 0.9 | 1.10 ± 0.02 | $21/2^- \rightarrow 17/2^-$ | $E2$ |
| 550.2 | 1 | 80.2 ± 0.8 | 0.90 ± 0.02 | $25/2^- \rightarrow 21/2^-$ | $E2$ |
| 613.7 | 1 | 53.1 ± 1.3 [d] | 0.92 ± 0.04 | $29/2^- \rightarrow 25/2^-$ | $E2$ |
| 663.0 | 1 | 30.5 ± 0.4 | 0.90 ± 0.05 | $33/2^- \rightarrow 29/2^-$ | $E2$ |
| 718.6 | 1 | 15.3 ± 0.6 [d] | 1.19 ± 0.12 | $37/2^- \rightarrow 33/2^-$ | $E2$ |
| 753.7 | 1 | 7.6 ± 0.3 | 0.92 ± 0.15 | $41/2^- \rightarrow 37/2^-$ | $E2$ |
| 796 | 1 | 4.3 ± 0.5 | | $(45/2^-) \rightarrow 41/2^-$ | $(E2)$ |
| 475.2 | $1s$ | 13.6 ± 1.1 [d] | 1.14 ± 0.34 | $37/2^- \rightarrow 33/2^-$ | $E2$ |
| 555.6 | $1s \rightarrow 1$ | 12.6 ± 0.7 [d] | 1.00 ± 0.09 | $37/2^- \rightarrow 33/2^-$ | $E2$ |
| 585.2 | $1s$ | 23.7 ± 1.9 [d] | 1.03 ± 0.16 | $41/2^- \rightarrow 37/2^-$ | $E2$ |
| 669.7 | $1s$ | 14.9 ± 0.5 | 1.16 ± 0.26 | $45/2^- \rightarrow 41/2^-$ | $E2$ |
| 742 | $1s$ | 7.4±0.3 | 1.22 ± 0.38 | $(49/2^-) \rightarrow 45/2^-$ | $(E2)$ |
| 743 | $1s \rightarrow 1$ | | | $33/2^- \rightarrow 29/2^-$ | $E2$ |
| 803 | $1s$ | <5 | | $(53/2^-) \rightarrow (49/2^-)$ | $(E2)$ |
| 315.1 | $1s \rightarrow 4$ | 9.9 ± 0.7 [d] | 0.73 ± 0.17 | $33/2^- \rightarrow 31/2^-$ | $M1+E2$ |
| 479.9 | $1s \rightarrow 4$ | 17.5 ± 1.2 [d] | 1.31 ± 0.31 | $37/2^- \rightarrow 33/2^-$ | $E2$ |
| 612.9 | $1s \rightarrow 4$ | 19.3 ± 2.1 [d] | 0.92 ± 0.10 | $33/2^- \rightarrow 29/2^-$ | $E2$ |
| 263.0 | $2 \rightarrow 3$ | 29.5 ± 0.3 | 0.98 ± 0.03 | $21/2^+ \rightarrow 17/2^+$ | $E2$ |
| 282.3 | 2 | 44.5 ± 0.4 | 0.94 ± 0.02 | $21/2^+ \rightarrow 17/2^+$ | $E2$ |
| 361.6 | 2 | 91.9 ± 0.9 | 1.06 ± 0.03 | $25/2^+ \rightarrow 21/2^+$ | $E2$ |
| 434.0 | 2 | 83.6 ± 0.9 | 1.10 ± 0.04 | $29/2^+ \rightarrow 25/2^+$ | $E2$ |
| 497.5 | 2 | 78.6 ± 0.8 | 0.98 ± 0.04 | $33/2^+ \rightarrow 29/2^+$ | $E2$ |
| 555.5 | 2 | 61.7 ± 1.6 [d] | 0.92 ± 0.03 | $37/2^+ \rightarrow 33/2^+$ | $E2$ |
| 611.2 | 2 | 42.6 ± 0.6 | 0.94 ± 0.04 | $41/2^+ \rightarrow 37/2^+$ | $E2$ |
| 666.0 | 2 | 21.0 ± 0.5 | 0.79 ± 0.15 | $45/2^+ \rightarrow 41/2^+$ | $E2$ |
| 719.8 | 2 | 13.0 ± 1.4 [d] | 0.87 ± 0.13 | $49/2^+ \rightarrow 45/2^+$ | $E2$ |
| 770 | 2 | 8.1 ± 0.3 | 0.84 ± 0.24 | $53/2^+ \rightarrow 49/2^+$ | $E2$ |
| 817 | 2 | <5 | | $(57/2^+) \rightarrow 53/2^+$ | $(E2)$ |
| 195.1 | $2 \rightarrow 3$ | 18.1 ± 0.2 | 0.64 ± 0.03 | $17/2^+ \rightarrow 15/2^+$ | $M1+E2$ |
| 383.4 | $2 \rightarrow 3$ | 44.3 ± 0.5 | 1.01 ± 0.05 | $17/2^+ \rightarrow 13/2^+$ | $E2$ |
| 206.1 | $2 \rightarrow 5$ | 1.2 ± 0.2 [d] | 0.68 ± 0.18 | $21/2^+ \rightarrow 19/2^-$ | E1 |
| 378.9 | $2 \rightarrow 1$ | 3.9 ± 0.3 [d] | 1.54 ± 0.32 | $21/2^+ \rightarrow 21/2^-$ | E1 |
| 102.1 | 3 | 12.2 ± 0.2 | 0.36 ± 0.03 | $7/2^+ \rightarrow 5/2^+$ | $M1+E2$ |
| 125.9 | 3 | 22.7 ± 0.2 | 0.45 ± 0.02 | $9/2^+ \rightarrow 7/2^+$ | $M1+E2$ |
| 148.8 | 3 | 37.7 ± 0.4 | 0.64 ± 0.03 | $11/2^+ \rightarrow 9/2^+$ | $M1+E2$ |
| 168.3 | 3 | 36.3 ± 0.4 | 0.62 ± 0.03 | $13/2^+ \rightarrow 11/2^+$ | $M1+E2$ |
| 188.2 | 3 | 35.1 ± 0.4 | 0.63 ± 0.04 | $15/2^+ \rightarrow 13/2^+$ | $M1+E2$ |
| 210.1 | 3 | 6.4 ± 0.6 [d] | | $19/2^+ \rightarrow 17/2^+$ | $M1+E2$ |
| 214.4 | 3 | 18.4 ± 1.1 [d] | 1.05 ± 0.27 | $17/2^+ \rightarrow 15/2^+$ | $M1+E2$ |
| 228.0 | 3 | 9.3 ± 0.2 | 1.03 ± 0.19 | $9/2^+ \rightarrow 5/2^+$ | $E2$ |
| 234.0 | 3 | 8.0 ± 0.1 | 0.76 ± 0.12 | $21/2^+ \rightarrow 19/2^+$ | $M1+E2$ |
| 246.9 | 3 | 7.8 ± 0.9 [d] | 0.69 ± 0.15 | $23/2^+ \rightarrow 21/2^+$ | $M1+E2$ |
| 261.0 | 3 | 5.1 ± 0.7 | 0.72 ± 0.35 | $25/2^+ \rightarrow 23/2^+$ | $M1+E2$ |
| 274.7 | 3 | 14.6 ± 0.2 | 0.95 ± 0.08 | $11/2^+ \rightarrow 7/2^+$ | $E2$ |
| 278.9 | 3 | 6.3 ± 0.8 [d] | 0.75 ± 0.12 | $27/2^+ \rightarrow 25/2^+$ | $M1+E2$ |
| 317.1 | 3 | 43.7 ± 0.4 | 1.00 ± 0.06 | $13/2^+ \rightarrow 9/2^+$ | $E2$ |
| 356.6 | 3 | 43.3 ± 0.7 | 1.11 ± 0.06 | $15/2^+ \rightarrow 11/2^+$ | $E2$ |
| 402.6 | 3 | 21.3 ± 0.3 | 1.13 ± 0.08 | $17/2^+ \rightarrow 13/2^+$ | $E2$ |
| 424.1 | 3 | 24.1 ± 1.3 [d] | 0.93 ± 0.09 | $19/2^+ \rightarrow 15/2^+$ | $E2$ |
| 443.8 | 3 | 11.9 ± 0.2 [d] | 1.05 ± 0.19 | $21/2^+ \rightarrow 17/2^+$ | $E2$ |
| 480.9 | 3 | 26.5 ± 2.6 [d] | 1.08 ± 0.10 | $23/2^+ \rightarrow 19/2^+$ | $E2$ |
| 508.2 | 3 | 16.7 ± 1.8 [d] | 1.38 ± 0.27 | $25/2^+ \rightarrow 21/2^+$ | $E2$ |
| 539.9 | 3 | 19.7 ± 0.4 | 0.78 ± 0.13 | $27/2^+ \rightarrow 23/2^+$ | $E2$ |

TABLE I. (*Continued*.)

| $E_\gamma$ (keV) [a] | Band | $I_\gamma$ [b] | $R_{\rm DCO}$ [c] | $J_i^\pi \rightarrow J_f^\pi$ | Multipolarity |
|---|---|---|---|---|---|
| 228.9 | 3→2 | 7.3 ± 0.7 [d] | | $19/2^+ \rightarrow 17/2^+$ | $M1+E2$ |
| 463.0 | 3→2 | 15.1 ± 1.4 [d] | 0.98 ± 0.16 | $21/2^+ \rightarrow 17/2^+$ | $E2$ |
| 124.1 | 4 | 25.5 ± 0.3 | 0.52 ± 0.04 | $11/2^- \rightarrow 9/2^-$ | $M1+E2$ |
| 163.4 | 4 | 48.7 ± 0.5 | 0.62 ± 0.03 | $13/2^- \rightarrow 11/2^-$ | $M1+E2$ |
| 180.1 | 4 | 45.8 ± 0.6 | 0.68 ± 0.04 | $15/2^- \rightarrow 13/2^-$ | $M1+E2$ |
| 200.1 | 4 | 45.3 ± 0.5 | 0.63 ± 0.05 | $17/2^- \rightarrow 15/2^-$ | $M1+E2$ |
| 214.8 | 4 | 47.8 ± 0.5 | 0.73 ± 0.04 | $19/2^- \rightarrow 17/2^-$ | $M1+E2$ |
| 231.1 | 4 | 40.8 ± 0.4 | 0.80 ± 0.06 | $21/2^- \rightarrow 19/2^-$ | $M1+E2$ |
| 244.0 | 4 | 38.4 ± 1.3 [d] | 0.77 ± 0.05 | $23/2^- \rightarrow 21/2^-$ | $M1+E2$ |
| 258.6 | 4 | 28.2 ± 0.3 | 0.86 ± 0.05 | $25/2^- \rightarrow 23/2^-$ | $M1+E2$ |
| 270.9 | 4 | 18.6 ± 0.2 | 0.62 ± 0.05 | $27/2^- \rightarrow 25/2^-$ | $M1+E2$ |
| 285.5 | 4 | 19.6 ± 0.2 | 1.00 ± 0.15 | $29/2^- \rightarrow 27/2^-$ | $M1+E2$ |
| 287.3 | 4 | 7.6 ± 0.2 | 1.27 ± 0.30 | $13/2^- \rightarrow 9/2^-$ | $E2$ |
| 297.6 | 4 | 16.9 ± 0.4 | 0.64 ± 0.10 | $31/2^- \rightarrow 29/2^-$ | $M1+E2$ |
| 310.6 | 4 | 8.2 ± 0.6 [d] | 0.79 ± 0.14 | $33/2^- \rightarrow 31/2^-$ | $M1+E2$ |
| 324.6 | 4 | 5.3 ± 0.6 [d] | 0.74 ± 0.26 | $35/2^- \rightarrow 33/2^-$ | $M1+E2$ |
| 335.9 | 4 | 6.5 ± 0.6 [d] | | $37/2^- \rightarrow 35/2^-$ | $M1+E2$ |
| 337.6 | 4 | 5.0 ± 0.6 [d] | | $43/2^- \rightarrow 41/2^-$ | $M1+E2$ |
| 339.7 | 4 | 5.3 ± 0.6 [d] | | $39/2^- \rightarrow 37/2^-$ | $M1+E2$ |
| 341.4 | 4 | 5.0 ± 0.6 [d] | | $41/2^- \rightarrow 39/2^-$ | $M1+E2$ |
| 343.5 | 4 | 18.3 ± 0.2 | 1.15 ± 0.12 | $15/2^- \rightarrow 11/2^-$ | $E2$ |
| 380.3 | 4 | 28.1 ± 0.7 [d] | 1.00 ± 0.10 | $17/2^- \rightarrow 13/2^-$ | $E2$ |
| 415.0 | 4 | 33.6 ± 0.4 | 1.09 ± 0.09 | $19/2^- \rightarrow 15/2^-$ | $E2$ |
| 446.0 | 4 | 48.6 ± 0.5 | 1.06 ± 0.09 | $21/2^- \rightarrow 17/2^-$ | $E2$ |
| 475.1 | 4 | 53.5 ± 4.4 [d] | 0.95 ± 0.07 | $23/2^- \rightarrow 19/2^-$ | $E2$ |
| 502.7 | 4 | 56.6 ± 4.6 [d] | 0.94 ± 0.08 | $25/2^- \rightarrow 21/2^-$ | $E2$ |
| 529.6 | 4 | 55.2 ± 1.0 | 0.95 ± 0.07 | $27/2^- \rightarrow 23/2^-$ | $E2$ |
| 556.4 | 4 | 50.1 ± 3.0 [d] | 0.88 ± 0.06 | $29/2^- \rightarrow 25/2^-$ | $E2$ |
| 583.2 | 4 | 40.1 ± 0.5 | 1.04 ± 0.17 | $31/2^- \rightarrow 27/2^-$ | $E2$ |
| 608.3 | 4 | 33.2 ± 2.2 | 0.94 ± 0.15 | $33/2^- \rightarrow 29/2^-$ | $E2$ |
| 635.3 | 4 | 23.0 ± 1.7 [d] | 0.87 ± 0.12 | $35/2^- \rightarrow 31/2^-$ | $E2$ |
| 660.3 | 4 | 11.7 ± 2.0 [d] | 1.23 ± 0.36 | $37/2^- \rightarrow 33/2^-$ | $E2$ |
| 666 | 4 | <7 | | $(45/2^-) \rightarrow 41/2^-$ | |
| 675.6 | 4 | 13.3 ± 0.4 | 1.18 ± 0.19 | $39/2^- \rightarrow 35/2^-$ | $E2$ |
| 679.2 | 4 | 8.9 ± 1.1 [d] | 0.91 ± 0.36 | $43/2^- \rightarrow 39/2^-$ | $E2$ |
| 681.2 | 4 | 7.8 ± 1.1 [d] | 0.88 ± 0.33 | $41/2^- \rightarrow 37/2^-$ | $E2$ |
| 140.0 | 4→1 | <3 | | $(9/2^- \rightarrow 9/2^-)$ | $(M1+E2)$ |
| 739 | 4→1 | <4 | | $(33/2^- \rightarrow 29/2^-)$ | |
| 655.7 | 4→1*s* | 7.3 ± 1.1 | 1.26 ± 0.38 | $37/2^- \rightarrow 33/2^-$ | $E2$ |
| 327.4 | 5 | <3 | | $15/2^- \rightarrow 11/2^-$ | $E2$ |
| 506.4 | 5 | 7.3 ± 0.7 [d] | 1.08 ± 0.11 | $23/2^- \rightarrow 19/2^-$ | $E2$ |
| 593.1 | 5 | 9.3 ± 0.5 [d] | 1.06 ± 0.13 | $27/2^- \rightarrow 23/2^-$ | $E2$ |
| 625.6 | 5 | 8.7 ± 0.8 [d] | 1.02 ± 0.13 | $31/2^- \rightarrow 27/2^-$ | $E2$ |
| 661 | 5 | 5.0 ± 1.4 [d] | | $(35/2^-) \rightarrow 31/2^-$ | $(E2)$ |
| 708 | 5 | <5 | | $(39/2^-) \rightarrow (35/2^-)$ | $(E2)$ |
| 431.3 | 5 | 8.1 ± 1.0[d] | | $19/2^- \rightarrow 15/2^-$ | $E2$ |
| 432.6 | 5→1 | | | $11/2^- \rightarrow 9/2^-$ | $M1+E2$ |
| 557.2 | 5→1 | <5 | | $15/2^- \rightarrow 13/2^-$ | $M1+E2$ |
| 638.1 | 5→1 | 10.1 ± 0.6 [d] | 0.40 ± 0.06 | $19/2^- \rightarrow 17/2^-$ | $M1+E2$ |
| 679.5 | 5→1 | 9.9 ± 1.1 [d] | 0.23 ± 0.10 | $23/2^- \rightarrow 21/2^-$ | $M1+E2$ |
| 722 | 5→1 | <5 | | $(27/2^- \rightarrow 25/2^-)$ | |
| 556.9 | 5→6 | 5.4 ± 0.8 [d] | | $27/2^- \rightarrow 23/2^-$ | $E2$ |
| 380.8 | 6 | 3.3 ± 0.4 [d] | 1.38 ± 0.32 | $19/2^- \rightarrow 15/2^-$ | $E2$ |
| 449.2 | 6 | 11.1 ± 0.2 | 1.05 ± 0.10 | $23/2^- \rightarrow 19/2^-$ | $E2$ |
| 480.4 | 6 | 5.7 ± 0.6 [d] | 1.06 ± 0.11 | $27/2^- \rightarrow 23/2^-$ | $E2$ |

TABLE 1. (*Continued.*)

| $E_\gamma$ (keV) [a] | Band | $I_\gamma$ [b] | $R_{DCO}$ [c] | $J_i^\pi \rightarrow J_f^\pi$ | Multipolarity |
|---|---|---|---|---|---|
| 551.0 | 6 | 6.9 ± 1.1 [d] | 0.99 ± 0.16 | $31/2^- \rightarrow 27/2^-$ | $E2$ |
| 606.6 | 6 | 3.2 ± 0.6 [d] | 1.24 ± 0.16 | $(35/2^-) \rightarrow 31/2^-$ | $E2$ |
| 631 | 6 | <4 | 1.04 ± 0.20 | $(39/2^-) \rightarrow (35/2^-)$ | $(E2)$ |
| 645 | 6→1 | 4.6 ± 0.7 [d] | | $27/2^- \rightarrow 25/2^-$ | $M1+E2$ |
| 701 | 6→1 | 2.9 ± 0.5 [d] | | $15/2^- \rightarrow 13/2^-$ | $M1+E2$ |
| 715 | 6→1 | <5 | | $23/2^- \rightarrow 21/2^-$ | $M1+E2$ |
| 731.3 | 6→1 | 8.7 ± 0.3 | 0.44 ± 0.14 | $19/2^- \rightarrow 17/2^-$ | $M1+E2$ |
| 516.3 | 6→5 | 8.3 ± 1.1 [d] | 1.15 ± 0.20 | $27/2^- \rightarrow 23/2^-$ | $E2$ |
| 336.8 | 7 | <5 | 1.75 ± 0.29 | ? | |
| 423.7 | 7 | 6.1 ± 0.7 [d] | 1.15 ± 0.10 | ? | |
| 466.0 | 7 | 4.0 ± 0.8 [d] | 1.03 ± 0.17 | ? | |
| 502.6 | 7 | 8.0 ± 0.9 [d] | 1.03 ± 0.10 | ? | |
| 602 | 7→1 | <5 | 1.01 ± 0.38 | $(? \rightarrow 13/2^-)$ | |
| 804.6 | 7→1 | <5 | | $? \rightarrow 9/2^-$ | |
| 938.6 | 7→1 | 7.7 ± 0.2 | | $? \rightarrow 13/2^-$ | |
| 1012 | 7→1 | 3.0 ± 0.3 | | $? \rightarrow 17/2^-$ | |

[a]Energy uncertainty for most of transitions ~ 0.2 keV, for those without decimal point ~ 0.5 keV.
[b,d]Intensities were obtained from the total projection spectrum and normalized with the transition 350.3 keV. However, for those contaminated peaks, as marked by [d], the results were taken from gated spectra.
[c]Blank space in the $R_{DCO}$ column indicates that no DCO ratio was able to be extracted for the transition.

Ir isotopes (see for example a summary by Nazarewicz *et al.* [22]). The assignment of band 1 to the decoupled $\pi h_{9/2}$ configuration agrees with the characteristics of the ground state band in this mass region and is consistent with the results in neighboring Ir isotopes [7,10,11,16]. The expected ground state $5/2^-$ is not observed in the experiment, but should lie very close to the $9/2^-$ state. Based on the systematics (e.g., 44 keV in $^{177}$Ir [7], 25 keV in $^{181}$Ir [10], 20 keV in $^{183}$Ir [16]), this energy in $^{179}$Ir should not exceed 40 keV.

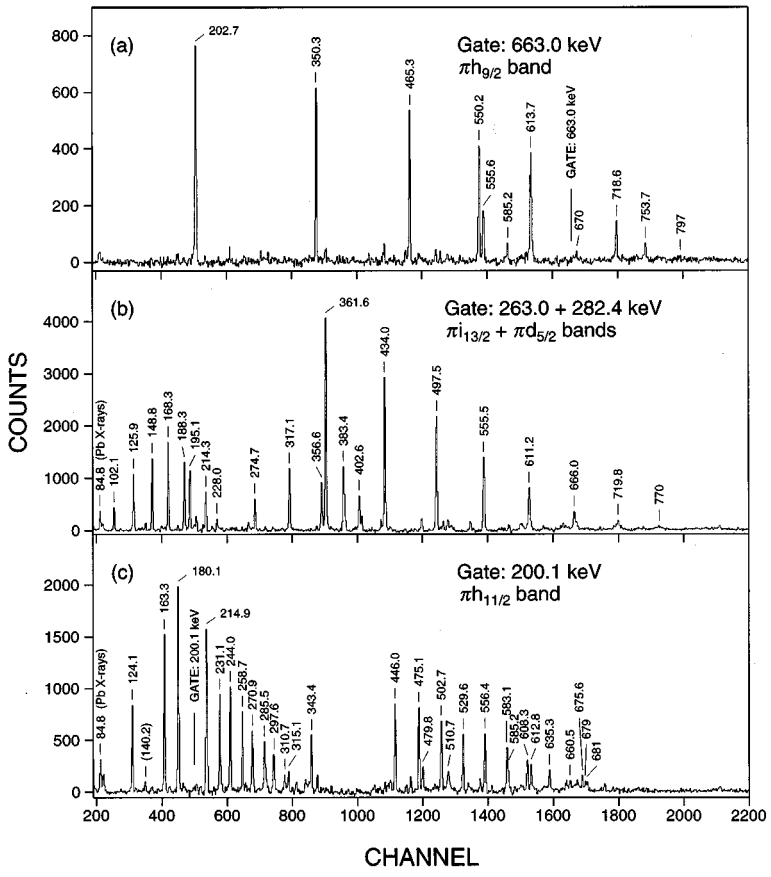


FIG. 2. Gated $\gamma$-ray spectra in $^{179}$Ir data: (a) on the 663.0-keV transition, (b) sum of 263.0 and 282.3 keV, and (c) on 200.1 keV.

Band 1*s* forms the yrast sequence above spin $33/2^-$ in band 1. The main intensity of band 1*s* branches into band 1 through a 555.6 keV transition to level $33/2^-$. The DCO data show that both the 555.6 ($37/2^-$ to $33/2^-$) and 743 ($33/2^-$ to $29/2^-$) keV transitions have quadrupole ($E2$) character although the latter one is contaminated by a similar transition at the top of band 1*s*. The transitions 718.6, 753.2, and 797 keV form the extension of the ground band, while band 1*s* was extended to spin ($53/2^-$), as the two branches demonstrated in Fig. 2(a). Similar features have been observed in the ground bands of many Os nuclei, for example $^{178,180}$Os [23] where both the ground-band extension and the *s* band were observed. Normally the yrast sequence is strongly populated in experiment, but in the gate of Fig. 2(a) this preference is not obvious. The phenomenon can be attributed to the competition of another branch from band 1*s* to band 4 (see Sec. III A 3) as well as from band 2.

#### *2. Bands 2 and 3*

The second strongest decay sequence observed in $^{179}$Ir is band 2 in which the 361.6-keV transition has a 91.9% relative intensity. This band mainly feeds into a strongly coupled band 3 through a few intense transitions. Apparently the bottom level in band 2 lies very close to one of the levels in band 3, resulting in two mixed levels at 1114.9 and 1134.1 keV. The complicated crossing pattern between bands 2 and 3 (see Sec. III C) can only occur if the two mixing levels have the same spin and parity since DCO ratios in Table I suggest $E2$ characteristics for the 263.0, 282.3, 443.8, and 463.0 keV transitions. The nice pattern of a rotational band [Fig. 2(b)] can be seen clearly up to 770 keV, while the last transition of 817 keV is tentative.

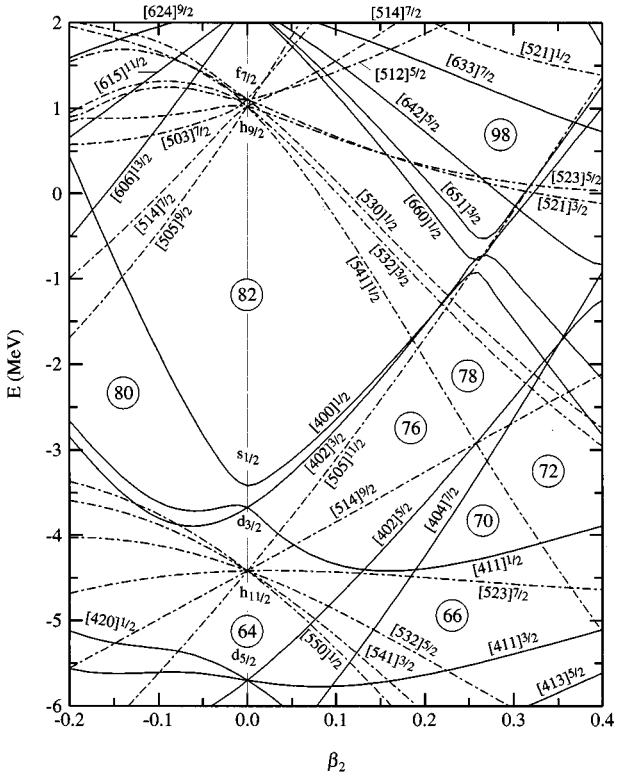


FIG. 3. Single-proton level diagram around $Z=77$ calculated with the Woods-Saxon potential by assuming $\beta_4=\gamma=0$.

Band 3 is a strongly coupled band, suggesting a high-$K$ configuration. Only one signature is observed in band 2, suggesting a low-$K$ structure with a large signature splitting, similar to band 1. Since bands 2 and 3 have the same parity, the logical association of Nilsson state for band 2 is the $1/2^+[660]$ ($\pi i_{13/2}$) orbital with its favored-signature sequence observed, and for band 3 is the $5/2^+[402]$ ($\pi d_{5/2}$) configuration (Fig. 3). The choice of negative parity orbitals is eliminated by the fact that only two weak transitions (206.1 and 378.9 keV) are observed connecting band 2 with the $\pi=-$ bands 1 and 5 (band 5 is discussed in Sec. III A 4).

The current assignment leads to an initial spin of $5/2^+$ for band 3. The two mixing levels at 1114.9 and 1134.1 keV then have spin $17/2^+$ and the 1397.2 keV level has spin $21/2^+$ which is consistent with the decays from this level to the $21/2^-$ in band 1 and $19/2^-$ in band 5. The bandhead of the $\pi i_{13/2}$ band should be $13/2^+$ but is not seen in the data since the mixing of the two $17/2^+$ states in bands 2 and 3 causes a major portion of the intensity in band 2 to feed into band 3 before reaching its bandhead. The large population intensity allows us to measure the lifetimes of states in the $\pi i_{13/2}$ band by using the Doppler shift attenuation method (DSAM) as described in Sec. III D. The intriguing behavior of the $\pi i_{13/2}$ band will be discussed in Sec. IV. The branching ratio analysis from the particle-rotor model in Sec. IV E 1 supports the assignment to band 3.

#### *3. Band 4*

Another strongly coupled structure, band 4, has been observed from spin $9/2^-$ up to ($45/2^-$). The determination of spin and parity for this band comes from the intriguing degeneracy of the two $33/2^-$ states in band 4 and band 1*s*. In fact they are only separated by 4.5 keV, and the overlap of wave functions of the two states leads to the observation of several interband transitions, just as those between bands 2 and 3. Band 4 is strongly populated in the experiment and shows no signature splitting. The most logical choice of assignment is the high-$K$ $\pi h_{11/2}$ band built on the $9/2^-[514]$ orbital, which systematically appears in the Ir isotopes (and is the ground structure in some Re nuclei). The measurements of interband transitions between bands 4 and 1*s* ensure the band assignment and particularly enable us to determine the bandhead energy which is very important in terms of discussing the relative Routhians.

The ''picket-fence'' structure of band 4 [Fig. 2(c)] enables us to extract the $B(M1;I\rightarrow I-1)/B(E2;I\rightarrow I-2)$ ratios. These ratios are very sensitive to the intrinsic structure of a band and the change due to band crossings. The results of the $B(M1)/B(E2)$ analysis and the application of the particle-rotor model to these data presented in Sec. IV E 1 confirm the above assignment to band 4. There is a possible transition (very weak 739-keV line) connecting the 2920.9-keV level of band 4 with the 2182.2-keV level of band 1. It relies on the fact that the 660.3 and 675.6-keV peaks were observed in the 613.7-keV gate of band 1. The top transition (666 keV) is also uncertain.

The bandhead $9/2^-$ state in band 4 must be isomeric since no transition to the $5/2^-$ ground state is observed, although a

weak transition (140 keV) from this state to the $9/2^-$ state of band 1 might exist [Fig. 2(c)]. The same situation occurs in band 3 where no obvious decaying-out transition is observed. Kaczarowski *et al.* [10] found that the corresponding $5/2^+$ and $9/2^-$ states in $^{181}$Ir are isomeric with $\tau_{1/2}=0.33\mu$ s and $\tau_{1/2}=0.13\mu$ s, respectively, while Dracoulis *et al.* [11] measured 430 ns and 193 ns. Apparently the lifetimes exceed the coincidence time window ($\sim$100 ns) in our experiment.

#### *4. Bands 5 and 6*

Two relatively weak rotational sequences (about 10% intensity level) were established as bands 5 and 6 in the level scheme of $^{179}$Ir. Both bands show similar structures, which are indicated by the similar decaying-out pattern into the lower levels of the ground $h_{9/2}$ band. Small DCO ratios (Table I) for the crossing transitions of 638.1, 679.5, and 731.3 keV suggest the $M1$ interband transition pattern (this means $\pi=-$) although the $E1$ possibility cannot be eliminated. An interlocking decay structure is observed between the two bands at levels 1697.5 and 1733.5 keV, suggesting the same spin and parity for the two levels and ensuring the same parity for bands 5 and 6.

Signature splitting is another point to be examined. Bands 5 and 6 show a decoupled structure like band 1 or 2. The low-$K$ requirement excludes the likelihood of $\pi=+$ states and leaves three possible candidates: $3/2^-[532]$, the unfavored signature of $1/2^-[541]$, and $1/2^-[530]$ from the $\pi f_{7/2}$ shell. Furthermore, the favored signature of $1/2^-[530]$ and the unfavored signature of $1/2^-[541]$ have the same value of $\alpha=-1/2$ and therefore the same spin sequence, while the favored sequence of $3/2^-[532]$ has the opposite signature of $\alpha=1/2$. The choice of the $3/2^-[532]$ configuration is automatically eliminated due to the same spin and parity preference of bands 5 and 6. Thus, the unfavored signature of $1/2^-[541]$ is assigned to band 5 and the favored signature of $1/2^-[530]$ to band 6. This assignment to band 6 fits very well into the signature-splitting systematics of the known $\pi h_{9/2}$ bands in Ir and Au nuclei [24–27], as shown in Fig. 4. The decrease of signature splitting in Au isotopes can be understood by the fact that the decoupled 1/2[541] state is further away from the Fermi surface.

The low-lying $\pi f_{7/2}$ band is observed for the first time in Ir nuclei. This $f_{7/2}$ structure has been identified in $^{185}$Au by Larabee *et al.* [26]. It is quite surprising to notice that the structures of the $\pi f_{7/2}$ bands in $^{179}$Ir and $^{185}$Au are so similar. For instance, in $^{185}$Au this band decays into the favored signature of the ground $\pi h_{9/2}$ band through a series of $M1$ transitions, and there is the crossing transition pattern between the $f_{7/2}$ band and the unfavored $h_{9/2}$ band occurring exactly at the same spin of $23/2^-$ as in $^{179}$Ir. The initial spin for the $f_{7/2}$ band is also $15/2^-$ but the excitation energy is less than that in $^{179}$Ir (776.1 keV versus 903.5 keV), which is understandable due to the two more protons in Au.

A systematic study of theoretically predicted bandheads in the rare-earth region by Nazarewicz *et al.* [22] have shown that the bandhead of the $f_{7/2}$ structure in odd-$A$ Ir and Au nuclei lowers in energy as the neutron number decreases, and reaches its lowest point around $N=102,104$. The calculated bandhead energy in $^{179}$Ir using the Woods-Saxon potential is about 510 keV ($7/2^-$ state) in comparison with $\sim$300 keV for $^{185}$Au. However, the calculations using the Nilsson potential with the standard ($\kappa$, $\mu$) parameters suggested by Bengtsson and Ragnarsson [28] cannot reproduce the data in this region very well, and particularly the predicted excitation energies for the $\pi f_{7/2}$ and $\pi i_{13/2}$ orbitals are too high in comparison with the experimental data. Zhang *et al.* [29] has suggested new sets of ($\kappa$, $\mu$) for the Au-Pt region based on the new experimental information from $^{185}$Au. Although it results from only one piece of experimental information, the new parameters do give better results in this region.

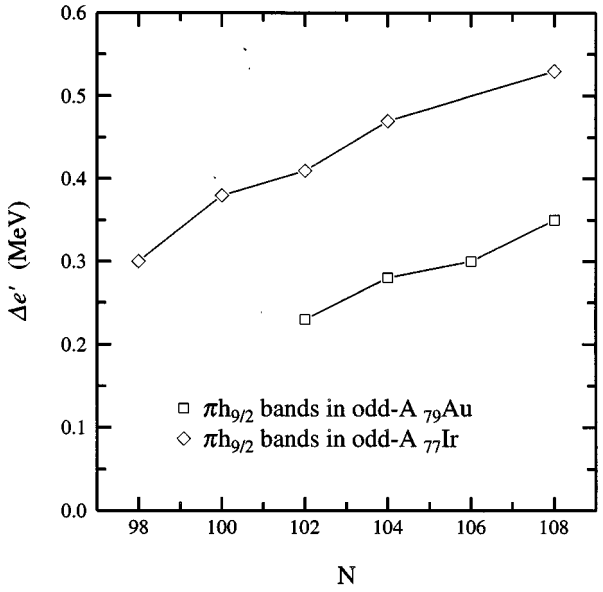


FIG. 4. Energy signature splitting for the known $\pi h_{9/2}$ bands in odd-$A$ Ir and Au nuclei at $\hbar\omega=0.22$ MeV. References are given in the text.

#### *5. Band 7*

The most uncertain assignment in the level scheme is band 7, which decays into the ground band via several transitions. Spins and parities for this band could not be assigned but the three transitions (423.7, 502.6, and 466.0 keV) have the $E2$ character from the DCO data. The DCO ratio (1.75 $\pm$0.29) for the 336.8-keV line seems to have no $E2$ character within the experimental error. No definite assignment to band 7 can be made from the current experiment but a couple of speculations are discussed here. One possible configuration might be a prolate band built on the $\pi h_{9/2}$ $3/2^-$ [532] Nilsson state with $I^\pi$ sequence of $7/2^-$, $9/2^-$, . . . . This needs the starting spin of band 7 to be measured. Another possible choice is an oblate band with the $\pi h_{9/2}$ orbital coupling to an oblate shape, as reported in Au and Pt decay work [30]. The oblate band in this case should be strongly coupled since the oblate core is coupled with a high-$K$ orbital from the $h_{9/2}$ shell. However, in our $^{179}$Ir experiment only one signature is observed and we would have to assume that the missing signature partner is due to its weak population.

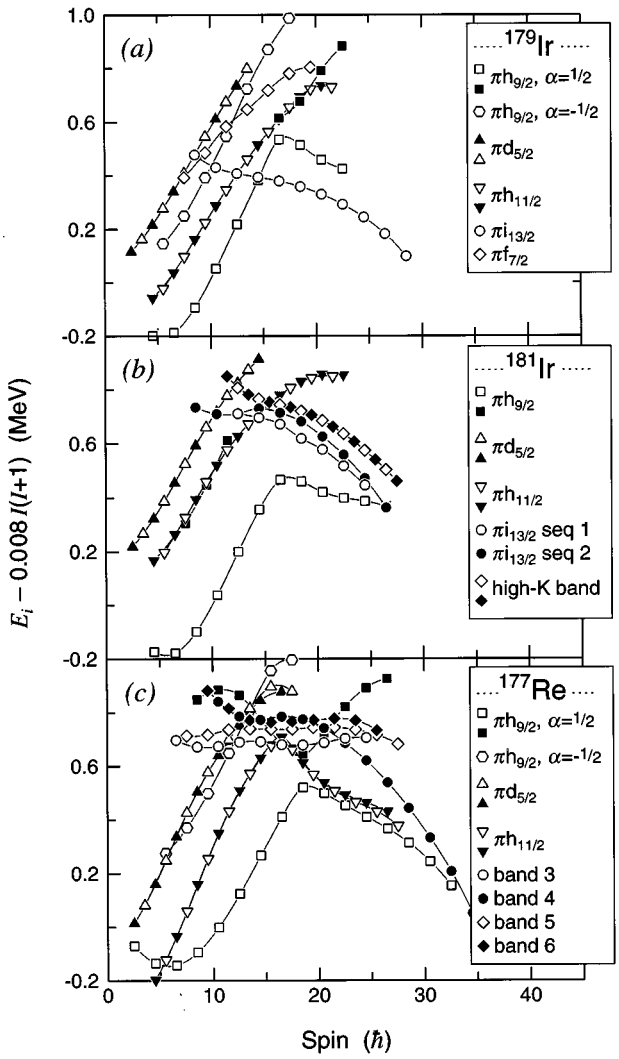


FIG. 5. Energies of levels relative to a rotating rigid core for observed bands in $^{179}$Ir (this work), $^{181}$Ir [11], and $^{177}$Re [9].

### B. Absence of other positive parity bands

Band 2 in $^{179}$Ir clearly has features that lead to its association with the $\pi i_{13/2}$ 1/2[660] orbital, including the absence of a signature partner, high initial quasiparticle alignment, and an enhanced transition quadrupole moment (see later sections in this paper). This is similar to the situation in the lighter Ir isotopes. However, close lying sets of positive parity bands are seen in $^{181}$Ir [11] and in $^{177}$Re [9]. This difference is illustrated in Fig. 5, which contains plots of the energies of the observed bands in $^{179}$Ir, $^{181}$Ir, and $^{177}$Re relative to a reference of a rigid rotor. In both $^{181}$Ir and $^{177}$Re there are close-lying positive parity bands in the 600 – 800 keV range (on the scale of Fig. 5) around $I = 15\,\hbar$, whereas in $^{179}$Ir we observe a single such band lower in energy, around 400 keV. As discussed by Bark *et al.* [9], these multiple positive parity bands in $^{175}$Re result from the coupling of $\pi h_{9/2}$ with negative parity two-neutron configurations, mixed with the 1/2[660] proton orbital. Only at higher spin in $^{177}$Re does the $\pi i_{13/2}$ character become more pure as it (band 4) separates from the other excitations and drops in energy. In $^{179}$Ir, the 1/2[660] orbital apparently comes lower in energy (due to a larger ground state deformation) compared to $^{181}$Ir, and thus our band 2 lies at 400 keV on the scale of Fig. 5. Presumably there exists another set of positive parity bands 300 keV higher in energy, analogous to those seen in $^{181}$Ir and $^{177}$Re. However, the 1/2[660] band in $^{179}$Ir is not significantly mixed with those higher-lying bands, due to the energy difference.

### C. Two-level mixing analysis in $^{179}$Ir

It is worthwhile to extend our discussion to one special feature in the level scheme of $^{179}$Ir — the interband transitions among six different bands. Four interband transitions (315.1, 479.8, 612.8, and 656 keV) have been observed between the $h_{9/2}$ yrast sequence and the strongly coupled $h_{11/2}$ band. It is surprising that the three $33/2^-$ states in these bands come so close in energy (different only by 80.4 and 4.5 keV, respectively), such that the $33/2^-$ in bands 1*s* and 4 are almost degenerate. The interaction matrix element can roughly be estimated by a two-level mixing scheme.

The mixed states $|\psi_1\rangle$ and $|\psi_2\rangle$ can be related to the two unperturbed states $|1\rangle$ and $|2\rangle$ by

$$|\psi_1\rangle = a|1\rangle + b|2\rangle,$$
$$|\psi_2\rangle = -b|1\rangle + a|2\rangle, \tag{1}$$

where $a$ and $b$ satisfy the normalization condition $a^2+b^2=1$. The relationship between the interaction matrix element $V$ and the perturbed energies ($E_1$, $E_2$) is then expressed as

$$|V| = ab(E_1-E_2) = a\sqrt{1-a^2}(E_1-E_2). \tag{2}$$

The coefficients $a$ and $b$ are directly related to the measured transition rates:

$$\frac{B(E2,\psi_0\rightarrow\psi_1)}{B(E2,\psi_0\rightarrow\psi_2)} = \frac{a^2}{b^2}, \tag{3}$$

where $|\psi_0\rangle$ is assumed to be a pure, unperturbed level.

The branching ratios can be extracted from the experimental data and the results are summarized in Table II. As one can see from the table, a very small interaction of $|V| = 2.2$ keV is obtained for the two $33/2^-$ states of bands 1*s* and 4. This can be understood due to the *K* forbiddenness between the $K = 1/2\ h_{9/2}$ and $K = 9/2\ h_{11/2}$ bands. However, because of the near degeneracy of the two $33/2^-$ levels, even small mixing of the wave functions allows the interband transitions to occur.

In $^{175}$Os, near degeneracy of rotational states at spin $25/2^-$ and $29/2^-$ in the $1/2^-[521]$ and $5/2^-[512]$ bands has been reported (Ref. [31]) and a very small interaction matrix element of about 4 keV has been suggested by a 25% difference in deformation between the two configurations. In $^{179}$Ir, the very small interaction between the $h_{11/2}$ band and three quasiparticle *s* band could also indicate substantial difference in deformation between them, whereas the ground $h_{9/2}$ band and *s* band show more closeness and stronger interaction ($|V| \sim 40$ keV in Table II). Jensen *et al.* [32] obtained the shape information from the analysis of interaction strength between the $\pi h_{11/2} 7/2^-[523]$ and $\pi h_{9/2}$ $1/2^-[541]$ configurations in $^{163}$Tm and a ratio of

TABLE II. Interaction matrix element $|V|$ extracted from a two-level mixing analysis for the $33/2^-$, $17/2^+$ and $23/2^-$ states in $^{179}$Ir.

| Level | Energy (keV) | Transition (keV) $\rightarrow E_1$ | Transition (keV) $\rightarrow E_2$ | $a^2/b^2$ | a | b | $\|V\|$ (keV) |
|---|---|---|---|---|---|---|---|
| $33/2^-$ | $E_1$: 2925.4 | 475.4 | 479.9 | $1.59\pm0.15$ | 0.79 | 0.62 | 2.2 |
| | $E_2$: 2920.9 | 655.7 | 660.3 | $1.64\pm0.21$ | | | |
| $33/2^-$ | $E_1$: 2925.4 | 475.4 | 555.6 | | | | $\sim 40$ |
| | $E_2$: 2845.2 | | | | | | |
| $17/2^+$ | $E_1$: 1134.1 | 263.0 | 282.3 | $0.94\pm0.02$ | 0.70 | 0.72 | 9.6 |
| | $E_2$: 1114.9 | | | | | | |
| $23/2^-$ | $E_1$: 1733.5 | 480.4 | 516.3 | $0.98\pm0.08$ | 0.71 | 0.71 | 18.0 |
| | $E_2$: 1697.5 | 556.9 | 593.1 | $1.00\pm0.11$ | | | |

$Q_t([541])/Q_t([523])\sim 1.2$ was given. In $^{179}$Ir the two $37/2^-$ levels in bands 1$s$ and 4 are far apart and relatively pure, thus no shape information for the $\pi h_{11/2}$ and $\pi h_{9/2}$ configurations could be given by such an analysis.

There is also a noticeable interaction between the two $17/2^+$ states in bands 2 ($K=1/2$) and 3 ($K=5/2$). The extracted interaction strength is 9.6 keV, understandably intermediate to the values mentioned in the two prior cases in the same level scheme. Another place where the level crossings occur is the two $27/2^-$ and $23/2^-$ states in bands 5 and 6. The relatively strong interaction ($V=18.0$ keV) is observed for the two $23/2^-$ states, indicating close structures preserved in the two configurations. This is consistent with the assignments of $\pi f_{7/2}$ $1/2^-[530]$ and $\pi h_{9/2}$ $1/2^-[541]$ to the two bands where both have the same signature $\alpha=-1/2$, parity and $K$ quantum number.

### D. DSAM lifetime measurements in $^{179}$Ir

Due to the strong population of the $\pi i_{13/2}$ band and the use of a backed target in the experiment, we were able to perform the lifetime measurements for states in the band by DSAM. The experimental condition is discussed in Sec. II. Line shapes were measured from spectra at five different detector angles and gated on transitions lying below the levels for which lifetimes are to be obtained. The quadrupole moments were fitted according to the method described in Ref. [33].

Monte Carlo simulated velocity distributions of the recoil nucleus in the target and backing were calculated for 3000 histories under the current beam-target-backing combination. During the calculation of line shapes from a given set of emitting and feeding states, the emitted yield at each time step is evaluated from the Bateman equations [33] and then the simulated shapes at each time step are added. The time step used in our analysis is 0.0075 ps which is small enough that the difference in line shape from step to step can be negligible.

The final line shapes were fitted in a least-squares fit procedure. Such a task for the DSAM lifetime analysis of $^{179}$Ir data was performed by a program (DSAMFT) developed by Gascon *et al.* [33]. There are several quantities that are treated simultaneously in the fitting process: (1) the transition quadrupole moment $Q_t$, (2) the transition quadrupole moment $Q_{ts}$ of the unobserved side feedings, (3) the intensity of the fitted peaks, (4) the linear background below the peaks, and (5) the intensity of contaminant stopped peaks. The data from five angles were fitted simultaneously, starting from the top of a band, and proceeding downward. The adopted parameters are those that minimize the $\chi^2$ of a fitting.

In a rotational band, the intensity of a transition in the band decreases as spin increases. This is due to the unobserved side-feeding transitions. The side-feeding cascade was simulated for each state by a three-level model with an effective moment of inertia of $60\hbar^2$/MeV. Side-feeding intensities were corrected according to the decrease of intensities in the band. The fitted results for the three states ($41/2^+$, $45/2^+$, and $49/2^+$) in the $\pi i_{13/2}$ band are given in Table III. The fitted line shapes together with the data for the 719.9-keV transition at five different angles are shown in Fig. 6. The averaged quadrupole moment from the three fitted states is $Q_t=7.74^{+1.98}_{-1.35}$ $e$ b. We also analyzed the lifetimes of states in the $\pi h_{9/2}$ band, however, no obvious line shapes could be seen. Only an upper limit of 6 $e$ b was estimated in this case. These results are consistent with those obtained [21] from the recoil distance method for the lower-spin states in both bands.

## IV. DISCUSSION OF RESULTS

Our discussions start with the alignment features observed in different configurations of the new data (Sec. IV A). The interpretation will concentrate on the role of intruder states, particularly the $\pi h_{9/2}$ and $\pi i_{13/2}$ orbitals (Secs. IV B–IV D). In Sec. IV E the applications of a particle-rotor model to the electromagnetic properties of $^{179}$Ir are presented.

TABLE III. Measured lifetimes and quadrupole moments for three states in the $\pi i_{13/2}$ band of $^{179}$Ir.

| Spin | $E_\gamma$ (keV) | $\tau$ (ps) | $Q_t$ ($e$ b) |
|---|---|---|---|
| $49/2^+$ | 719.8 | $0.20^{+0.07}_{-0.06}$ | $7.75^{+1.44}_{-1.12}$ |
| $45/2^+$ | 666.0 | $0.26^{+0.14}_{-0.10}$ | $8.17^{+2.19}_{-1.51}$ |
| $41/2^+$ | 611.2 | $0.51^{+0.32}_{-0.20}$ | $7.30^{+2.30}_{-1.41}$ |

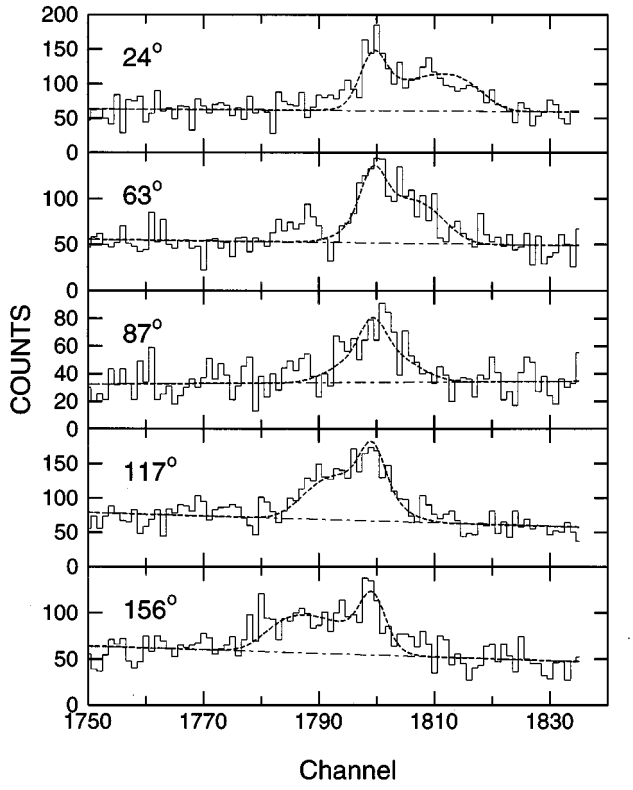


FIG. 6. The line shapes and the DSAM lifetime fitting results for the 719.2-keV transition in the $\pi i_{13/2}$ band in $^{179}$Ir. Spectra from $\gamma$-ray detectors in five different angle groups are shown.

### A. Alignments in $^{179}$Ir

The alignment and backbending phenomenon in different bands can be seen from the usual plot [34] of aligned angular momentum $i$ as a function of rotational frequency $\hbar\omega$ in Fig. 7, where the collective rotational contribution is subtracted out. The Harris parameters $\mathcal{J}_0$ ($=22\hbar^2$/MeV) and $\mathcal{J}_1$ ($=90\hbar^4$/MeV$^3$) were chosen such that the alignment curve of the $\pi h_{9/2}$ band before the band crossing is flat. The obvious observation is that a sharp backbending occurs at

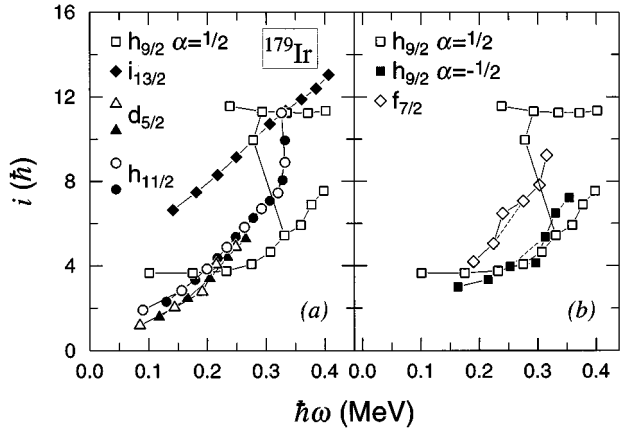


FIG. 7. Aligned angular momentum as a function of rotational frequency for bands in $^{179}$Ir. The Harris parameters are chosen to be $\mathcal{J}_0=20\hbar^2$/MeV and $\mathcal{J}_1=90\hbar^4$/MeV$^3$ such that the rotating reference for the $\pi h_{9/2}$ band is subtracted.

$\hbar\omega_c=0.3$ MeV in the $h_{9/2}$ band. Backbending is usually caused by the alignment of a broken pair of high-$j$ quasiparticles. In the rare-earth region, the first band crossing has been well understood due to the $\nu i_{13/2}$ alignment (referred to as the $AB$ crossing), although in the Ir-Pt-Au region evidence of the $\pi h_{9/2}$ alignment [15, 16] has been shown. The observed backbending in the $\pi h_{9/2}$ band in Ir nuclei is naturally associated with the $\nu i_{13/2}$ alignment, whereas the $\pi h_{9/2}$ alignment is blocked. The alignment gain is about $6.5\hbar$, consistent with fact that the neutron Fermi surface is in the middle of the $i_{13/2}$ shell and only half of the full $i_{13/2}$ alignment is present.

In contrast a smooth gain in alignment as a function of frequency occurs in most other bands, when the $h_{9/2}$ band is used as a reference. Such a smooth aligning process extends to relatively high spin in the $\pi i_{13/2}$ and $\pi h_{11/2}$ bands. The same feature has been observed in other odd-$A$ Ir nuclei (e.g., Refs. [5–7, 10, 11, 15]). There are several aspects to be considered in the following subsections for the increase of alignment: increase of moment of inertia due to larger deformation or pairing reduction, shape changing, and/or quasiparticle aligning. An upbending around $\hbar\omega\sim0.31$ MeV seems forming at the last few points in the $\pi h_{11/2}$ band in $^{179}$Ir. As in Sec. IV E, the measured $B(M1)/B(E2)$ ratios suggest that this upbending could be associated with a $\nu i_{13/2}$ alignment.

In Fig. 7(b) for $^{179}$Ir a ''bump'' occurs about $\hbar\omega\sim0.25$ MeV (spin 23/2 to 27/2) in the alignment curve of the $f_{7/2}$ band, while a ''dip'' happens in the curve of the $\alpha=-1/2$ signature of the $h_{9/2}$ band. Such a phenomenon is due to the interaction between the two $23/2^-$ states of the two bands (Fig. 1), which pushes the two levels away from each other. A similar interaction can be seen between the $d_{5/2}$ band and the $i_{13/2}$ band at spin 17/2 in Fig. 7(a).

### B. Deformation driving of intruder states

The deformation driving effect of an intruder can be viewed as core polarization from a particle occupying the orbital. Such a force is magnified when the orbital is far away from the Fermi surface. An example is the $\nu i_{13/2}$ state in $A=130$ region where the Fermi surface for neutrons is below the $i_{13/2}$ shell. Studies by the Stony Brook group [1] show that in $^{137}$Sm ($N=75$) the 1/2[660] ($\nu i_{13/2}$) band has 50% larger moment of inertia than the yrast $h_{11/2}$ band does and the potential energy surface calculations indicate a significantly larger deformation in the $i_{13/2}$ band. This observation was confirmed [35] by lifetime measurements. The role of proton intruders, $\pi h_{9/2}$ and $\pi i_{13/2}$, is similar in many aspects.

#### *1. The $\pi h_{9/2}$ bands*

As an indirect measurement of nuclear deformation, we can examine the frequency of the $\nu i_{13/2}$ backbend occurring in different bands. The band crossing frequency is directly related to the quasiparticle energy at $\omega=0$:

$$\sqrt{(\epsilon_\nu-\lambda)^2+\Delta^2},$$

where $\epsilon_\nu$ is the single particle energy, $\lambda$ is the Fermi level energy, and $\Delta$ is the pairing gap. Clearly the pairing gap and

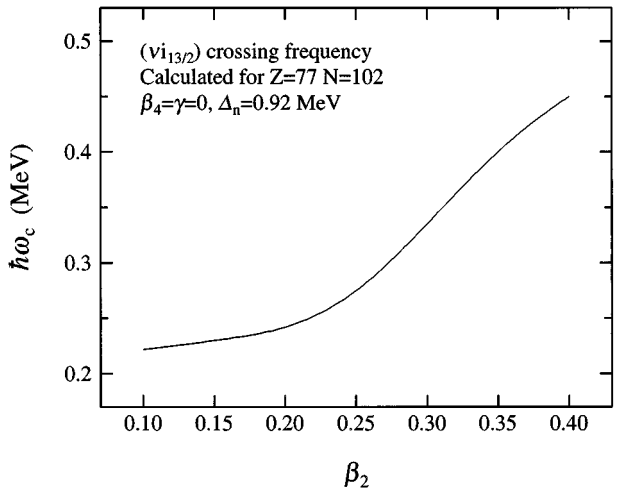


FIG. 8. Calculated $\nu i_{13/2}$ crossing frequency as a function of $\beta_2$ deformation for $Z=77$, $N=102$, $\beta_4=\gamma=0$, and $\Delta=0.92$ MeV.

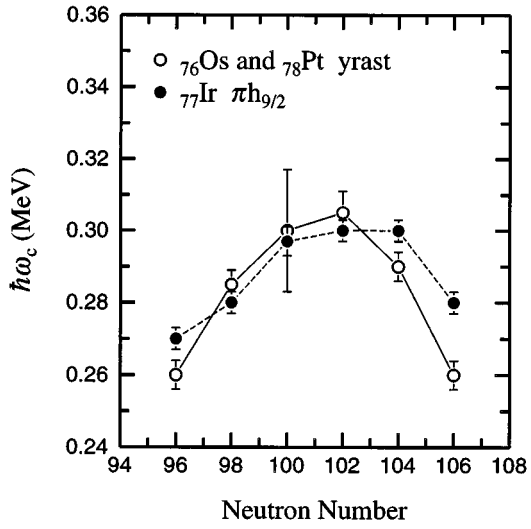


FIG. 9. Measured crossing frequencies for $\nu i_{13/2}$ alignment for $\pi h_{9/2}$ bands in Ir isotopes (dotted line) compared to the values for the even-even cores of these nuclei (solid line).

Fermi surface location play crucial roles, the latter factor depending directly on deformation. As the quadrupole deformation increases, based on cranked shell model calculations, the band crossing shifts to higher rotational frequency, as illustrated in Fig. 8.

The intruder $\pi h_{9/2}$ bands have been observed from $Z=67$ (Ho) up to many $_{77}$Ir and $_{79}$Au nuclei. Analogous to the case of the $\nu i_{13/2}$ state in $^{137}$Sm, the proton Fermi surface in Ho is below the $\pi h_{9/2}$ shell. Experimentally the delay of the $\nu i_{13/2}$ crossing in $\pi h_{9/2}$ bands has been reported in a series of odd-$Z$ odd-$A$ nuclei from Ho to Ta (see, e.g., [8, 33, 36, 37]). One can at least qualitatively attribute the shifts to the larger deformation of the nucleus in the intruder $\pi h_{9/2}$ band. However, Gascon *et al.* [33] have measured lifetimes by the DSAM technique in $^{157}$Ho and found that there is not enough enhancement in the $B(E2)$ value in the $\pi h_{9/2}$ band to totally account for the large delay in the $\nu i_{13/2}$ crossing frequency. Recently Sun *et al.* [38] demonstrated the importance of including quadrupole pairing in calculations for the delayed crossing frequency.

On the other hand, in Ir nuclei no shift of this $\nu i_{13/2}$ crossing frequency in the $\pi h_{9/2}$ bands is observed relative to the average of the two adjacent even-even nuclei, as shown in Fig. 9. Such a change can be understood by considering the single-particle diagram of Fig. 3. There is a rather large gap in the single-particle spectrum at $Z=76$, and the occupation of the 77th proton in the 1/2[541] orbital has rather similar structure as the average of Os ($Z=76$) and Pt ($Z=78$) cores. This is to say that the proton Fermi surface moves into the $\pi h_{9/2}$ shell, and the intruder characteristics or core polarization of the $h_{9/2}$ orbital is largely lost.

#### 2. Intruder $\pi i_{13/2}$ bands

Due to its larger angular momentum, the $i_{13/2}$ proton intruder state should have more profound shape-driving characteristics than the $\pi h_{9/2}$ state. Bands built on the $\pi i_{13/2}$ state have been established in a number of Au [24–27], Ir [5–7], and Re [2–4] nuclei. The bands have been observed down to the 13/2 bandhead in Au isotopes but only to the 17/2 member in most Ir and Re nuclei.

Similarities of the observed $\pi i_{13/2}$ bands in Ir and Re nuclei can be seen from the alignment diagram, as compared

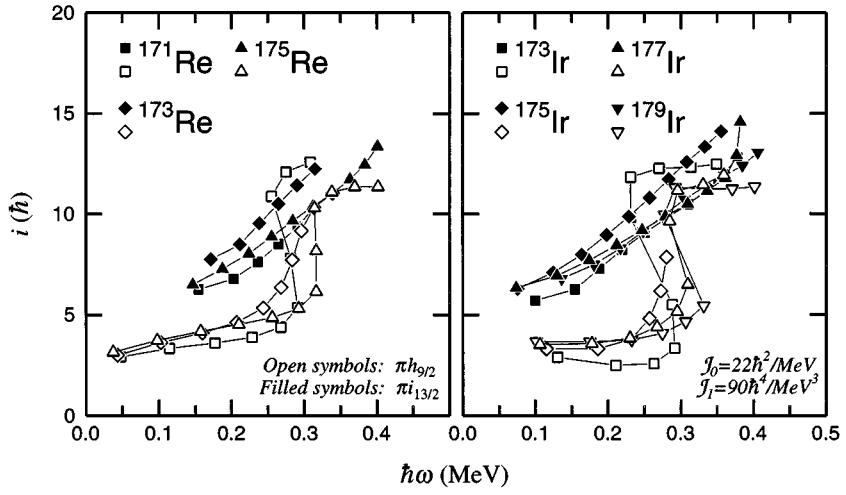


FIG. 10. Aligned angular momentum as a function of rotational frequency for the observed $\pi i_{13/2}$ bands in Re (left) and Ir (right) isotopes. The $\pi h_{9/2}$ bands are plotted as a comparison. References are given in the text.

to the corresponding $\pi h_{9/2}$ bands in Fig. 10. A sharp backbending is present in all the $\pi h_{9/2}$ bands, while only a smooth gradual gain in alignment is exhibited in the $\pi i_{13/2}$ bands (up to the experimentally observed frequency limit). The comparison between the $\pi i_{13/2}$ state and the $\pi h_{9/2}$ state in Ir nuclei is very much similar to the $\nu i_{13/2}$ vs $\nu h_{11/2}$ in $A=130$ region and the $\pi h_{9/2}$ vs $\pi h_{11/2}$ in the lighter rare-earth nuclei (e.g., $^{157}$Ho [33] and Lu [36]).

Evidence of large deformation in the $\pi i_{13/2}$ band has been indicated by TRS calculations (next section), which predict $\beta_2 \sim 0.3$ for this configuration and $\beta_2 \sim 0.23$ for the $\pi h_{9/2}$ band in $^{179}$Ir. The more direct evidence of an enhanced deformation comes from the measured quadrupole moments in $^{179}$Ir as discussed in Sec. III D. The average $Q_t$ measured for three states ($41/2^+$, $45/2^+$, and $49/2^+$) in the 1/2[660] band is about 7.7 $e$ b. By comparison, there are no observable line shapes on any transition in the $\pi h_{9/2}$ band in $^{179}$Ir, where only an upper limit of 6 $e$ b can be given. The approximate relationship between $Q_t$ and the quadrupole deformation $\beta_2$ of an axially symmetric nucleus before band crossing is [39]

$$Q_t = 0.0109 Z A^{2/3} \beta_2 (1 + 0.36\beta_2). \tag{4}$$

Therefore, for different bands in the same nucleus, the ratio of the quadrupole moments is roughly equal to the ratio of $\beta_2$ values. In $^{179}$Ir, the deformation of the $\pi i_{13/2}$ configuration is 20–30 % larger than that of the $\pi h_{9/2}$ band. The dominant cause of the smooth alignment gain in the $i_{13/2}$ bands is the substantial difference of deformation between it and the band ($\pi h_{9/2}$) used to define the reference, i.e., improper Harris parameters ($\mathcal{J}_0$ and $\mathcal{J}_1$) used in the plot for the $\pi i_{13/2}$ band. Lifetime measurements with the recoil distance method on several low-spin states in $^{181}$Ir by Kaczarowski *et al.* [40] and in $^{179}$Ir by Müller *et al.* [21] have given a similar conclusion.

The large deformation in the $\pi i_{13/2}$ state also causes the delay of the $\nu i_{13/2}$ crossing in the band. Another consequence of large $\beta_2$ (= 0.3) in the $\pi i_{13/2}$ band is that the $Z=76$ proton gap is no longer present in the single-particle diagram in Fig. 3. In such a region the level density is large and the difference between Ir ($Z=77$) and Re ($Z=75$) nuclei is small, as indicated by the similarity of alignments in Fig. 10.

### C. Configuration-dependent shapes

The influence of intruder states on nuclear shapes has been studied theoretically from the total Routhian surfaces (TRS's). These are deformation self-consistent Strutinsky-Bogolyubov cranking calculations using a nonaxial Woods-Saxon potential. Deformation parameters included are ($\beta_2$, $\gamma$, $\beta_4$) and the total Routhian (or energy) is minimized with respect to the parameter $\beta_4$ in a ($\beta_2, \gamma$) plane. For a thorough description of TRS calculations in the $A=180$ region one can refer to the work of Wyss *et al.* [41].

In the TRS calculations two quantum numbers, parity $\pi$ and signature $\alpha$, are used to label four different configuration groups: $A(+,+1/2)$, $B(+,-1/2)$, $E(-,-1/2)$, and $F(-,+1/2)$. To determine a quasiparticle configuration associated with an energy minimum in the TRS map, one can use the calculated deformation parameters to perform the standard cranked shell model (CSM) calculation and identify the lowest quasiparticle state in the Routhian diagram.

TABLE IV. Deformations ($\beta_2$, $\gamma$, $\beta_4$) predicted in TRS calculations for one-quasiparticle configurations in $^{179}$Ir and the yrast configuration in $^{178}$Os at different rotational frequencies.

| $\hbar\omega$ (MeV) | $\beta_2$ | $\gamma$ | $\beta_4$ |
|---|---|---|---|
| | $^{179}$Ir $\pi, \alpha = +, +1/2$ | | |
| 0.091 | 0.293 | 1.65 | 0.006 |
| 0.171 | 0.296 | 1.61 | 0.005 |
| 0.211 | 0.297 | 1.50 | 0.005 |
| | $^{179}$Ir $\pi, \alpha = +, -1/2$ | | |
| 0.091 | 0.258 | −0.01 | −0.007 |
| 0.171 | 0.266 | −0.21 | −0.006 |
| 0.211 | 0.271 | −1.49 | −0.003 |
| | $^{179}$Ir $\pi, \alpha = -, +1/2$ | | |
| 0.091 | 0.228 | 2.19 | −0.012 |
| 0.171 | 0.233 | 3.14 | −0.013 |
| 0.211 | 0.238 | 2.49 | −0.012 |
| | $^{179}$Ir $\pi, \alpha = -, -1/2$ | | |
| 0.091 | 0.254 | −4.43 | −0.008 |
| 0.171 | 0.257 | −3.28 | −0.003 |
| 0.211 | 0.263 | −2.50 | −0.004 |
| | $^{178}$Os Yrast configuration | | |
| 0.050 | 0.228 | −0.63 | −0.016 |
| 0.091 | 0.233 | −0.87 | −0.014 |
| 0.171 | 0.258 | −0.66 | −0.009 |
| 0.212 | 0.271 | −0.60 | −0.005 |

Results of calculated deformations ($\beta_2$, $\gamma$, $\beta_4$) at three different rotational frequencies for four one-quasiproton configurations in $^{179}$Ir are listed in Table IV. For comparison the calculated values for the yrast configuration in the even-even $^{178}$Os core are also given in the table. A large $\beta_2 = 0.3$ is shown for the $(+,+1/2)$ configuration, primarily the $i_{13/2}$ state, in contrast to $\beta_2 = 0.23$ for the $(-,+1/2)$ $h_{9/2}$ state. The deformations of the $d_{5/2}$ and $h_{11/2}$ excitations in $^{179}$Ir (see the $\alpha=-1/2$ columns in Table IV) are nearly 20% larger than the value for the $h_{9/2}$ state.

Larger $\beta_2$ calculated for the $d_{5/2}$ and $h_{11/2}$ bands than for the $h_{9/2}$ band can be related to the fact that a pair of protons occupy the downsloping $\pi h_{9/2}$ orbital, while a hole is formed in an upsloping ($d_{5/2}$ or $h_{11/2}$) orbital, both serving to increase the deformation. Comparison of the Ir $h_{9/2}$ state with the Os core shows that the initial deformations at $\hbar\omega \sim 0.05$ MeV for both cases are similar. This is a consequence of the Fermi level in the $h_{9/2}$ shell.

TRS calculations show a very large change of $\beta_2$ from $\hbar\omega = 0.05$ MeV to 0.21 MeV for $^{178}$Os. The shape changing is believed to be responsible for the anomalous increase of moments of inertia in the yrast bands of many even-even Os nuclei. The physical origin of shape changes in Os nuclei is

due to the ''scattering'' of a pair of particles from an up-sloping orbital ($h_{11/2}$) to an opened down-sloping orbital ($h_{9/2}$) with the increase of rotational frequency, as pointed out by Dracoulis *et al.* [13] and Bengtsson *et al.* [14]. The probability of transferring or ''pair scattering'' to an opened orbital is very much dependent on how close this orbital is to the Fermi surface. This feature has been discussed in $^{171}$Re by Bark *et al.* [2].

The deformation driving effect from the neutron shell, which influences the location of the Fermi level, will have a large impact on the probability of proton pair scattering in even-even and odd-$A$ nuclei. In Ir nuclei $\beta_2$ reaches a maximum around $N=102$ in the middle of the shell, while towards either side of $N$ the deformation is decreasing. The systematic study of shape changes from TRS calculations [41] demonstrates such a trend. In $^{179}$Ir it is likely that the largest contribution from the neutron shell leads to the formation of a hole excitation in the $\pi h_{11/2}$ and $\pi d_{5/2}$ states even at very low rotational frequency.

It should be pointed out that in the lighter Pt nuclei ($N \leqslant 98$) an irregular alignment pattern in the yrast band of $^{176}$Pt ($N=98$) has been attributed to shape coexistence [42, 43]. This phenomenon corresponds to the initial occupation of the last two protons in the $11/2^-[505]$ orbital or in the mixed $d_{3/2}$ $3/2^+[402]$ and $s_{1/2}$ $1/2^+[401]$ level (Fig. 3). At higher rotational frequency, the probability to occupy the $h_{9/2}$ orbital becomes larger and a shape shift from small deformation to large deformation is predicted [43] by the calculation. A similar phenomenon has been reported in $^{173}$Ir ($N=96$) by Juutinen *et al.* [5] and led to an assignment of the $11/2^-[505]$ configuration to the observed band.

Bark, Bengtsson, and Carlson [44] have recently performed calculations on the shape evolution in the $\pi h_{9/2}$ and $\pi i_{13/2}$ bands in Re and Ir nuclei. Using the ultimate cranker code (based on the Nilsson potential), they come to a different conclusion on deformations in the $\pi i_{13/2}$ band compared to the results shown in Table IV. They propose that the deformation in the $\pi i_{13/2}$ band begins at a value similar to that for the $\pi h_{9/2}$ band ($\epsilon_2 \approx 0.23$) and gradually increases to a value of 0.29 before the $\nu i_{13/2}$ crossing decreases the $\epsilon_2$ value to that found low in the band. This corresponds to a $\beta_2$ range of $0.24 - 0.30$ as a function of spin or rotational frequency, whereas our total Routhian surface calculations indicate a much more constant value of $\beta_2 \approx 0.29 - 0.30$. As discussed by Bark *et al.*, this difference is related to the probability of occupation of a proton pair in the 1/2[541] orbital over this frequency or spin range using these two potentials (Woods-Saxon for the TRS calculation and Nilsson for the ultimate cranker code). In their calculations, this orbital gains population only at the higher values of spin, whereas in our TRS results a pair is in the $\pi h_{9/2}$ orbital at the lowest frequencies. Although the uncertainties on the measured lifetimes in the $\pi i_{13/2}$ band in $^{179}$Ir (our results coupled with those of Müller *et al.* [21]) are not small enough to conclude whether the transition quadrupole moment is constant as a function of spin or increasing, the difference in the transition quadrupole moments of the $\pi h_{9/2}$ and $\pi i_{13/2}$ bands is still evident.

### D. Band crossings and CSM calculations

One way to explain a gradual alignment gain (such as in bands $\pi d_{5/2}$ and $\pi h_{11/2}$ of $^{179}$Ir) is a band crossing with large interaction strength. In the Ir-Pt-Au region it is a fact that the Fermi surface enters the proton $h_{9/2}$ shell and the competition of the $(\pi h_{9/2})^2$ alignment is expected. The question is how much this process contributes to the behavior of alignment in Ir nuclei. Evidence suggests [26, 45] that alignment features in $^{185}$Au and $^{184}$Pt result from the existence of two band crossings ($\nu i_{13/2}$ and $\pi h_{9/2}$) at nearly degenerate frequencies. Furthermore, Janzen *et al.* [15] presented even stronger spectroscopic evidence [$B(M1)/B(E2)$ ratios] that both of these alignment processes occur below $\hbar\omega = 0.30$ MeV in $^{183}$Ir and $^{185}$Pt, although a different scenario has been suggested by Carpenter *et al.* [45]. Kreiner *et al.* [16] also pointed out the possibility of the $\pi h_{9/2}$ crossing from study of odd-odd nuclei.

To test the scenario of band crossings, we performed standard cranked shell model (CSM) calculations. As already known for some time, there are discrepancies between the predicted crossing frequencies and experimental data. Nonetheless we can at least obtain a general view about the systematic deviations of theory in comparison with the data.

The CSM calculations were performed with Woods-Saxon potential at a given deformation and pairing gap. Deformation parameters were taken from TRS calculations at $\hbar\omega \sim 0.17$ MeV (before the first band crossing). This is appropriate to reflect the nuclear shape in the crossing region as long as the deformation does not change too much before and after the band crossing. The full pairing gaps ($\Delta_0$) were chosen to be the empirical odd-even mass differences. This choice ensures only systematic errors but not random. In the calculation, 80% of the full pairing was used for a system with an even number of nucleons since we are dealing with vacuum and two-quasiparticle states; 70% was used for an odd nucleon system to count the extra reduction from the unpaired nucleon. A better treatment of the pairing gap could be to perform pairing self-consistent calculations with particle number projection.

#### *1. Results of ($\nu i_{13/2}$) crossings*

Experimentally the $\nu i_{13/2}$ crossing points are well-defined in $\pi h_{9/2}$ bands and both experimental crossing frequencies $\hbar\omega_c$ and interaction strength $V_{\rm expt}$ can be determined. For a qualitative or pattern comparison a crude estimation of experimental $V_{\rm expt}$ is obtained by the slope $\Delta\omega/\Delta i$ in the alignment diagram around the crossing point. Then $V_{\rm expt} < 0$ indicates a sharp backbending or small interaction strength, while $V_{\rm expt} > 0$ corresponds to a smooth aligning process or large interaction strength.

The theoretical crossing frequency $\hbar\omega_c$ and the interaction strength $V$ are obtained from the quasiparticle Routhian diagram, as illustrated in Fig. 11 for the case of the $\pi h_{11/2}$ configuration in $^{179}$Ir. The interaction strength is taken to be half of the distance between crossing Routhians, as illustrated by the arrows in the figure. Figure 12(a) shows the calculated and measured $\hbar\omega_c$ for $\nu i_{13/2}$ crossing in the $\pi h_{9/2}$ and $\pi h_{11/2}$ bands in Ir nuclei. The larger $\beta_2$ for the $\pi h_{11/2}$ compared to $\pi h_{9/2}$ band in $^{179}$Ir results in a predicted 0.011 MeV delay in the $\nu i_{13/2}$ frequency. The measurements on $^{179}$Ir indicate a 0.025 MeV delay, which must be considered as good agreement. The CSM calculations generally underestimate the neutron crossing frequencies by

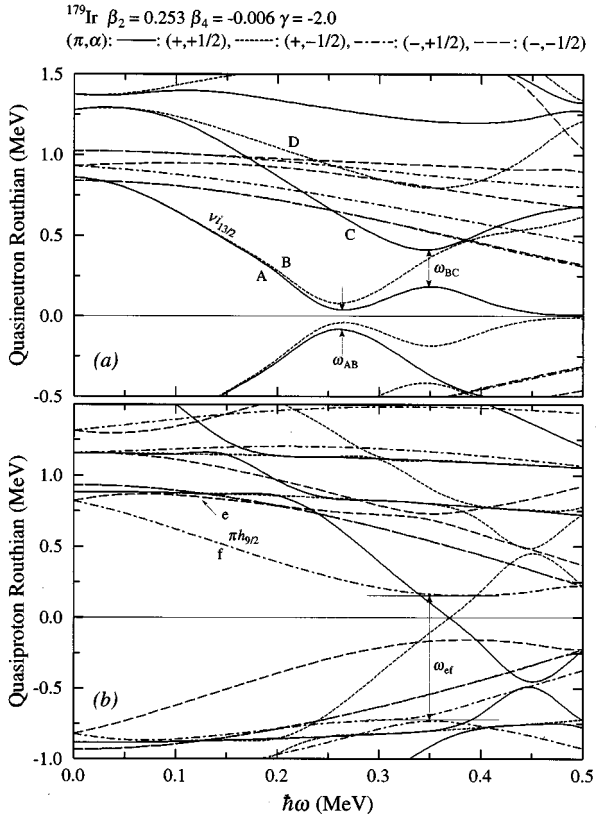


FIG. 11. Quasiparticle Routhians calculated from the cranked shell model. Deformation parameters are taken from the TRS results for the $\pi h_{11/2}$ configuration in $^{179}$Ir.

30–60 keV in comparison with the experimental observations in this region, however the overall trend is correctly shown. The experimental and theoretical interaction strengths are qualitatively compared in Fig. 12(b). The predicted pattern of interaction strength matches well with the data. For example, both theoretical and experimental $V$ values show a peak at $N=98$ and a dip at $N=96,102$. It is important to notice that the calculated $V$ values are small, around 150 keV, indicating backbendings in experiment.

### 2. Results of ($\pi h_{9/2}$) crossings

The experimental $\pi h_{9/2}$ crossing has not been well established, only clear evidence of this crossing having been reported in $^{187}$Au [27]. It results from a fact that the expected $\nu i_{13/2}$ crossing does not occur in the $\pi h_{9/2}$ band until possibly $\hbar\omega = 0.38$ MeV, while a sharp backbending shows at $\hbar\omega = 0.23$ MeV in the $\pi i_{13/2}$ band of $^{187}$Au.

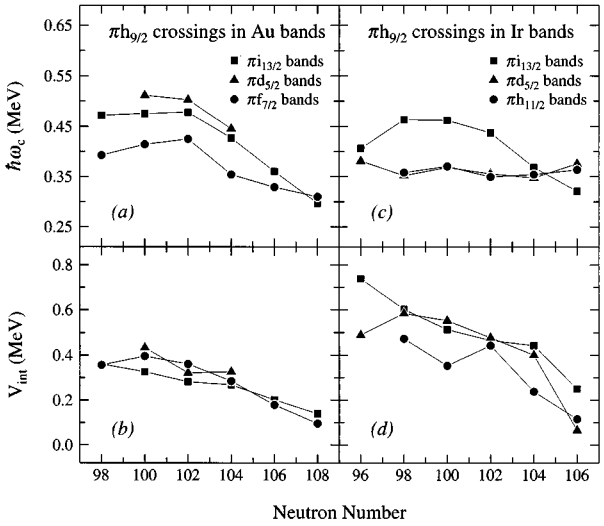


FIG. 13. Predicted crossing frequencies and interaction strength from the CSM calculations for the $\pi h_{9/2}$ alignment in Au (a) and (b) and Ir (c) and (d) nuclei.

In order to make a comparison with the experiment, we included a series of Au isotopes in our calculations as well as Ir isotopes. The calculated $\pi h_{9/2}$ crossing frequencies and interaction strengths are plotted in Fig. 13. Note that the $\pi h_{9/2}$ crossing frequency ($\hbar\omega = 0.30$ MeV) is lowest in the Au isotopes for $A=187$, and the interaction strength ($V=140$ keV) is smallest (i.e., a backbend). The corresponding neutron crossing occurs at a higher frequency of $\hbar\omega = 0.35$ MeV. This agrees very well with what observed in the data for $^{187}$Au. As discussed by Carpenter *et al.* [45] the conditions for a low-frequency $\pi h_{9/2}$ crossing are just right in $^{187}$Au. The proton pairing is reduced by blocking in an odd-$Z$ nucleus; the $\pi i_{13/2}$ orbit drives the nucleus to larger $\beta_2$ and positive values of $\gamma$, both of which lower the $\pi h_{9/2}$ crossing frequency; the $\beta_4$ value is most negative for $^{187}$Au.

Although the calculations give the right order of crossing frequencies, it is clear that the theory underestimates $\hbar\omega_c$ for

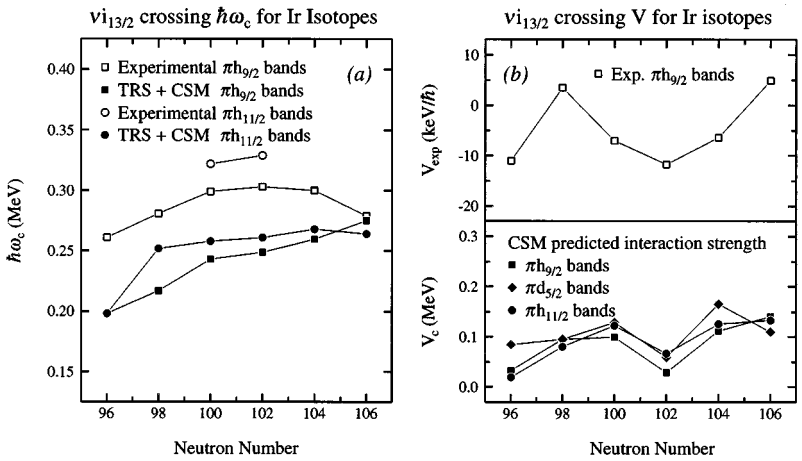


FIG. 12. (a) Crossing frequencies for $\nu i_{13/2}$ alignment plotted vs $N$ for the $\pi h_{9/2}$ and $\pi h_{11/2}$ bands in Ir nuclei. The calculated values are shown with a filled symbol, the measured with an open symbol. (b) Comparison of the pattern of $V_{expt}$ with those calculated from the cranked shell model.

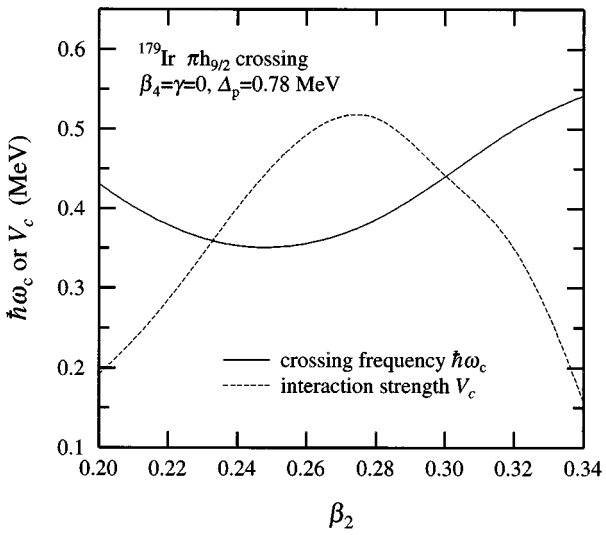


FIG. 14. Calculated crossing frequency and interaction strength for $\pi h_{9/2}$ alignment as a function of quadrupole deformation $\beta_2$ in $^{179}$Ir.

neutron crossings and overestimates it for proton crossings, in this case by 50–70 keV. On the other hand, the calculated interaction strength (140 keV) is very much in agreement with the pattern in the $\pi i_{13/2}$ band of $^{187}$Au.

In Ir isotopes the calculation indicates a $\pi h_{9/2}$ crossing of higher frequency (0.35 MeV) and much larger interaction strength (0.4–0.5 MeV) in the $\pi d_{5/2}$ and $\pi h_{11/2}$ bands, as shown in Figs. 13(c) and (d). This large interaction $V$ for a $\pi h_{9/2}$ crossing in $^{179}$Ir is demonstrated in Fig. 11(b). The $i$ vs $\hbar\omega$ diagram for $^{179}$Ir (Fig. 7) indicates a gradual rise in alignment in these two bands, an effect which is not present in the $\pi h_{9/2}$ band. If we take into account the $\hbar\omega_c$ shifts between theory and experiment in $^{187}$Au, the proton crossing could happen as early as $\hbar\omega \sim 0.3$ MeV in $^{179}$Ir with a large interaction strength. Therefore, the proton $h_{9/2}$ crossing may have a profound influence on the alignment pattern of the $d_{5/2}$ and $h_{11/2}$ bands in $^{179}$Ir.

CSM calculations also indicate that in the heavier Ir isotopes ($N \sim 106$) the $\pi h_{9/2}$ crossing frequency in the $d_{5/2}$ band reduces slightly to 0.33 MeV and the interaction strength decreases quickly to about 0.2 MeV. The neutron crossing is predicted about 0.3 MeV with interaction strength of 0.14 MeV in this case, which is very close to the $\pi h_{9/2}$ crossing. Janzen *et al.* [15] has reported a low-frequency $\pi h_{9/2}$ crossing in the $d_{5/2}$ band of $^{183}$Ir based on the $B(M1)/B(E2)$ measurements. This agrees with our conclusion.

Deformation plays a very important role in determining the proton $h_{9/2}$ crossing. Figure 14 illustrates calculated $\hbar\omega_c$ for the $\pi h_{9/2}$ crossing as a function of $\beta_2$ in $^{179}$Ir. At $\beta_2 \sim 0.25$, the crossing frequency reaches the lowest point (0.35 MeV) and the interaction strength becomes very large; at small or large $\beta_2$, $\hbar\omega_c$ increases and $V_c$ decreases. In $^{179}$Ir, $\beta_2$ is 0.25 – 0.26 for $h_{11/2}$ or $d_{5/2}$ bands, which is just in the proper range of deformation for a low $\pi h_{9/2}$ crossing frequency. Positive $\gamma$ and negative $\beta_4$ values can also bring down the proton crossing frequency as well as interaction strength, as shown in the case of $^{187}$Au. The blocking of proton pairing $\Delta_p$ from the extra proton can reduce the $h_{9/2}$ crossing frequency.

### E. Branching ratios and particle-rotor model

The pattern of transitions established in the strongly coupled bands in $^{179}$Ir enables us to measure the $B(M1)/B(E2)$ branching ratios within the bands. These rates are very sensitive to the single-particle configuration (reflected in the $g_K$ factor) and the quadrupole moment ($Q_0$) associated with a band. Theoretically within the framework of a particle-rotor model (PRM) we can test the spin and parity assignments in our newly observed data by comparing level structures and transition rates. Evidence for shape coexistence or an alignment process that is associated with the smooth increases in alignment in the $\pi h_{11/2}$ and $\pi d_{5/2}$ bands may be addressed from such a model.

We adopted the approach of the PRM described in Refs. [46,47]. The Woods-Saxon potential was used in our calculations and deformation parameters for single-particle states were taken from the TRS calculations.

The experimental $B(M1;I\rightarrow I-1)/B(E2;I\rightarrow I-2)$ ratios were extracted according to

$$\frac{B(M1;I\rightarrow I-1)}{B(E2;I\rightarrow I-2)} = 0.693\frac{E_\gamma^5(I\rightarrow I-2)}{E_\gamma^3(I\rightarrow I-1)}\frac{1}{\lambda(1+\delta^2)}(\mu/e\,\mathrm{b})^2, \quad (5)$$

where $E_\gamma$ are $\gamma$-ray energies in MeV, $\lambda$ is the $E2$ to $M1$ branching ratio [$=T(I\rightarrow I-2)/T(I\rightarrow I-1)$], and $\delta$ is the $E2/M1$ mixing ratio in the $\Delta I=1$ transition. The mixing ratio $\delta$ requires more detailed measurements, normally determined from the angular distribution data. Although the mixing ratio could be measured from the DCO ratios, the results are usually not very reliable due to large experimental uncertainties. Therefore, in the following discussions, we assume $\delta=0$ when extracting $B(M1)/B(E2)$ values. The $\delta$ values for the $d_{5/2}$ band in $^{183}$Ir [15] were measured ranging from 0.07 to 0.30, and their effect $(1+\delta^2)$ on the $B(M1)/B(E2)$ ratios is less than 10%. Therefore, $\delta=0$ in our discussions is a reasonable assumption.

#### *1. B(M1)/B(E2) ratios*

The experimental $B(M1)/B(E2)$ ratios for the two strongly coupled bands ($h_{11/2}$ and $d_{5/2}$) in $^{179}$Ir are plotted as symbol points in Figs. 15(a) and (b), respectively. The interactions between the $d_{5/2}$ and $i_{13/2}$ bands at spin $17/2^+$ and between the $h_{11/2}$ and $h_{9/2}$ bands at spin $33/2^-$ (see the level scheme in Fig. 1) were corrected in calculating $B(M1)/B(E2)$ ratios.

It appears that at low spin the magnitude of $B(M1)/B(E2)$ is about 1.7 for the $h_{11/2}$ band and about 0.8 for the $d_{5/2}$ band. Qualitatively this is consistent with the fact that the $h_{11/2}$ band has a larger $j$ value and $K$ value at its bandhead, thus a larger $g$ factor. The ratios gradually decrease as spin increases, and become roughly constant for quite some spin values where the alignment plots show constant increases. The $d_{5/2}$ band does not go much higher in spin, whereas the $B(M1)/B(E2)$ ratios of the $h_{11/2}$ band suddenly increase at the last two points (although with large error-bars).

In the PRM calculation, the deformation parameters were taken to be the larger $\beta_2$ set ($\beta_2=0.26$, $\beta_4=-0.004$, $\gamma=0$) suggested by Bengtsson [14]. The even-even core was treated as an effective rotor with its moments of inertia estimated from the deformation by the Grodzins' relation [39]. Pairing was treated in the standard BCS approach and gave a pairing gap of $\Delta_{\rm BCS}=1.187$ MeV. All Nilsson orbitals within 2.5 MeV of the Fermi level were included in the model space, and no Coriolis attenuation was used. The effective $g_s$ factor of the odd proton was taken as 70% of the free nucleon value, and the simple estimate of $Z/A$ was adopted for the core value, $g_R$. The calculated $B(M1)/B(E2)$ ratios are shown as solid lines for the $\pi h_{11/2}$ band in Fig. 15(a) and for the $\pi d_{5/2}$ band in Fig. 15(b).

The theoretical results agree very well with the experimental $B(M1)/B(E2)$ values in both cases up to fairly high spins. The sudden increase of the $B(M1)/B(E2)$ values at the last two points in the $h_{11/2}$ band coincides with the sharp upbend seen in the alignment plot [Fig. 7(a)]. Qualitatively, an increase in the $B(M1)$ values is consistent with an alignment of $i_{13/2}$ neutrons [48], and such a core rearrangement is not included in the particle-rotor model. In addition, a shape change to smaller $\beta$ and some triaxiality is predicted to accompany the neutron alignment (see Ref. [14]), which would decrease the $B(E2)$ values and thus also increase the $B(M1)/B(E2)$ ratios.

For the $\pi 5/2[402]$ band, part of the drop in the calculated $B(M1)/B(E2)$ ratios is due to the Coriolis mixing with the 7/2[404] band which is expected to lie rather close in energy. Although the 7/2[404] band has not been located in $^{179}$Ir, it has been identified recently in $^{175}$Re [4], where the importance of this mixing was pointed out and the strength of the mixing could be fitted to observed interband and intraband transitions. In the present calculations, the 7/2[404] component accounts for approximately 10% of the wave function at low spins, and about 28% at $I=23/2$, which is nearly identical to the fitted mixings reported in Ref. [4]. Thus, if the 7/2[404] band can be located in $^{179}$Ir, strong interband transitions (7/2[404] $\rightarrow$ 5/2[402]) should be expected here as well.

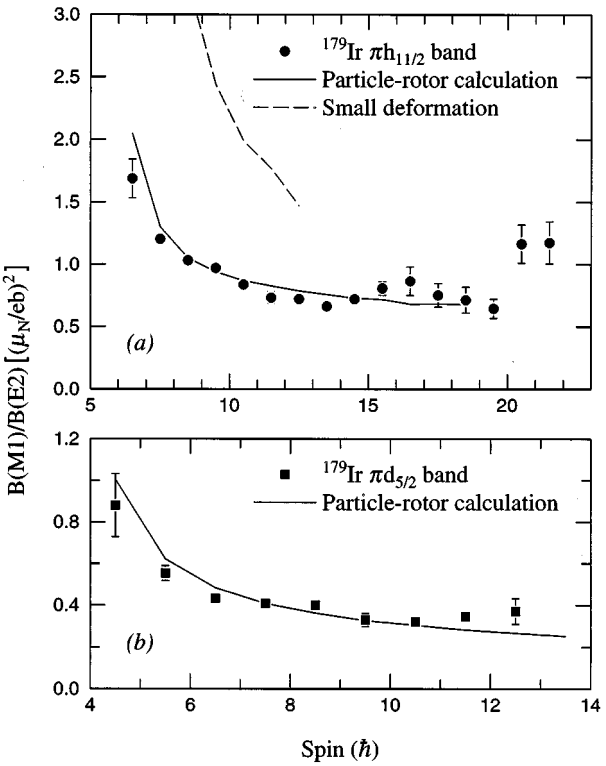


FIG. 15. Extracted $B(M1)/B(E2)$ ratios as symbol points for (a) the $\pi h_{11/2}$ band, (b) the $\pi d_{5/2}$ band in $^{179}$Ir. The results of particle-rotor model calculations are plotted as lines.

### *2. Test of different shapes in $^{179}$Ir*

In $^{179}$Ir, there have been suggested [14] two possible prolate deformations for the negative parity $h_{11/2}$ band: one at smaller $\beta_2\sim 0.19$ and one at larger $\beta_2\sim 0.26$. Such small deformation has led to an assignment [6] of the $11/2^-[505]$ configuration to a strongly coupled band observed in $^{175}$Ir, and consequently the shape change from the small deformation to the large one has contributed to the gradual gain of alignment in the band.

To test the two deformation conditions in $^{179}$Ir, we also performed the particle-rotor calculations with a smaller deformation parameter set ($\beta_2=0.19, \gamma=0, \beta_4=-0.02$). The predicted level structures for the negative parity states in $^{179}$Ir are shown in Fig. 16 (the upper one for the large deformation as given in the previous subsection and the lower one for the small deformation). The calculated $B(M1)/B(E2)$ values under the smaller deformation condition are also plotted in Fig. 15(a) as dashed line.

The calculations show that in the case of large deformation the decoupled $1/2^-[541]$ band is present as the ground configuration and the $9/2^-[514]$ state is excited at about 130 keV, which gives the right order in comparison with the data (Fig. 1). On the other hand, for the second deformation, the $11/2^-[505]$ is predicted to be the lowest configuration and both $1/2^-[541]$ and $9/2^-[514]$ are higher in energy, which is completely different from the experimental observation in Fig. 1. In particular, the $B(M1)/B(E2)$ ratios from the small deformation start with a value above 5 units, much larger than the extracted value ($\sim 1.7$). Clearly the model calculations support the assignment of the $9/2^-[514]$ hole state to band 4 in $^{179}$Ir, possessing large deformation ($\beta_2=0.26$).

The current $B(M1)/B(E2)$ data cannot show any clear evidence of the $\pi h_{9/2}$ crossing, which in contrast to the $\nu i_{13/2}$ crossing should decrease the $B(M1)$ value. However, if there is any crossing with large interaction strength, the $g_R$ factor gets renormalized over a large range of angular frequency and the contribution to $B(M1)/B(E2)$ should be very small. One last point: the PRM calculation shows the existence of the $1/2^-[530]$ band and the calculated energies are very close to those experimentally observed in $^{179}$Ir.

The above applications of the particle-rotor model were demonstrated at the Hands-on Nuclear Structure Theory Workshop at Oak Ridge [49]. Similar calculations with Woods-Saxon potential were reported for the $\pi h_{11/2}$ band in $^{181}$Ir in Ref. [50]. Their results are consistent with ours in $^{179}$Ir.

## V. CONCLUSION

In summary, rotational bands built on various quasiproton states have been established for the previously unknown nucleus $^{179}$Ir.

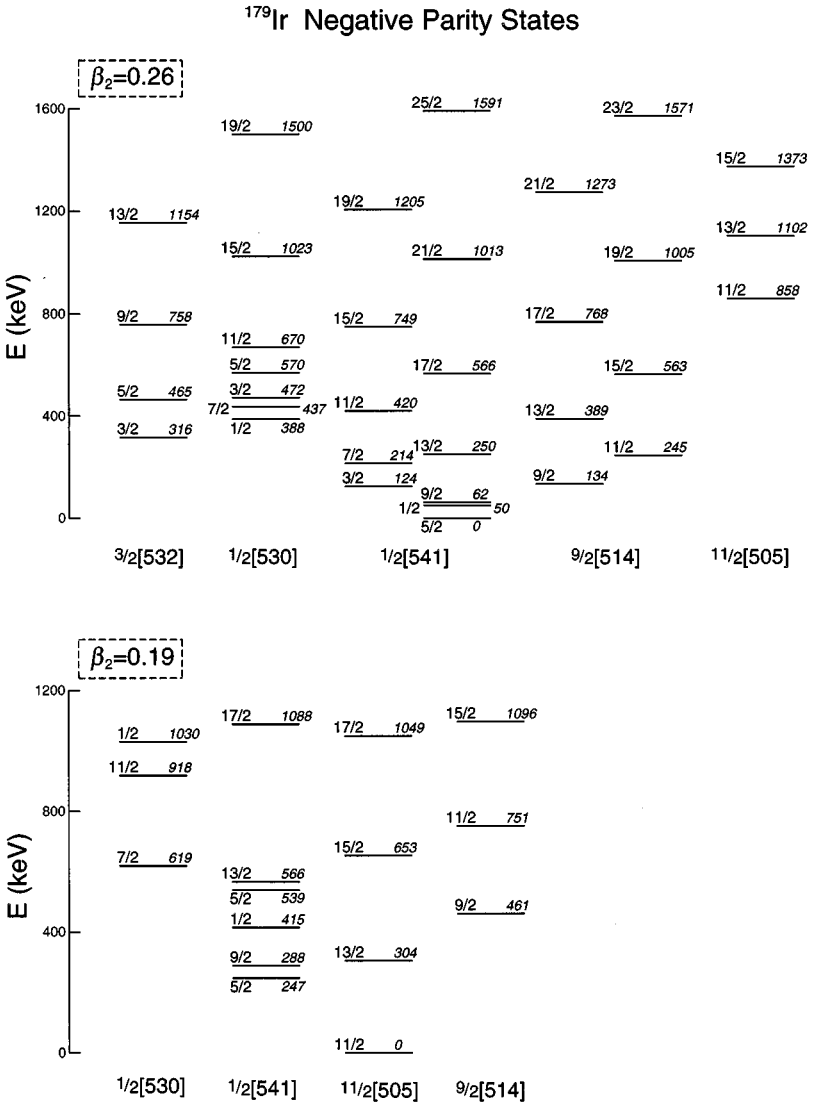


FIG. 16. Predicted level structure for the negative parity bands in $^{179}$Ir under two different deformation conditions, as deduced from particle-rotor model calculations.

The $\pi f_{7/2}$ ($1/2^-[530]$) band in $^{179}$Ir was identified for the first time in Ir nuclei. The primary focus of our study has been on the alignment feature observed in different configurations. This has further led us to investigate the role of intruder states in terms of three manifestations that are Fermi-surface dependent.

(1) *Deformation driving*. If the Fermi surface is low compared to the high-$j$ intruder state, then the excited band built on this orbital will exhibit significantly larger deformation or core polarization than other quasiparticle excitations in the same nucleus. It is found that the $h_{9/2}$ orbital retains its core polarization in the rare-earth region while in Ir nuclei the effect vanishes. In contrast the $\pi i_{13/2}$ orbital in Ir nuclei exhibits large deformation driving, indicated both from the lifetime measurements and the TRS calculations.

(2) *Shape changing*. If the Fermi surface is near the intruder state, then pairs of nucleons may be ''scattered'' into these orbitals, leading to larger deformations for many excitations in the nucleus or perhaps a shape change. It is likely that in $^{179}$Ir the largest deformation driving from the neutrons at middle shell ($N=102$) favors a hole configuration in both the $\pi h_{11/2}$ and $\pi d_{5/2}$ bands with a pair of protons in the down-sloping $\pi h_{9/2}$ orbital, resulting in larger deformation than that of the $\pi h_{9/2}$ band. The assumption of large deformation is supported by the particle-rotor model calculations.

(3) *Quasiparticle alignment*. If the Fermi surface is within the intruder shell, then rotational alignment of pairs of quasiparticles in the intruder orbitals is expected. It has been illustrated that the cranked shell model calculations underestimate the $\nu i_{13/2}$ crossing frequencies by 30–50 keV in comparison with the experimental data, and overestimate the $\pi h_{9/2}$ crossings by the same amount. The calculated interaction strength for the $\pi h_{9/2}$ crossing in $^{179}$Ir is about 450 keV in contrast to only $\sim$100 keV for the $\nu i_{13/2}$ crossing. Under these observations it is possible that both the $(\nu i_{13/2})^2$ and $(\pi h_{9/2})^2$ alignments contribute to the large range of alignment gain in the $\pi h_{11/2}$ and $\pi d_{5/2}$ bands in $^{179}$Ir.

The existence of a proton $h_{9/2}$ crossing is still a controversial issue. The systematic discrepancy of crossing frequencies is apparent between the experimental data and the conventional CSM calculations. This could be due to in CSM (1) inadequate parameters used to calculate the single-particle levels; (2) a necessity of including the quadrupole pairing. In fact, Sun *et al.* [38] have included the quadrupole pairing in the angular momentum projection theory and successfully explained the anomalous neutron crossing fre-

quency in odd proton rare-earth nuclei. Experimentally it would be very useful in future measurements: (1) to push the levels in $^{179}$Ir to even higher spin so that one could resolve the puzzle of band crossings in both the $\pi i_{13/2}$ and $\pi h_{11/2}$ bands; (2) to perform accurate lifetime or $g$-factor measurements on the states in different bands (particularly $\pi d_{5/2}$, $\pi h_{11/2}$, and $\pi i_{13/2}$), which would give direct information on nuclear shapes and band crossings.

## ACKNOWLEDGMENTS

We wish to acknowledge very fruitful discussions with R. Bengtsson, J.D. Garrett, W. Nazarewicz, and R. Wyss. The authors are most grateful to R. Wyss for help on the TRS calculations. The authors also wish to thank Y.S. Chen for valuable discussions. Research at the University of Tennessee is supported by the U.S. Department of Energy under Contract DE-SG05-87ER40361. Oak Ridge National Laboratory is operated by Martin Marietta Energy Systems Inc. under Contract DE-ACO5-84OR21400 with DOE. Partial support was also provided under DOE Contract DE-FG05-92ER40694. The Joint Institute for Heavy Ion Research is operated by the University of Tennessee, Vanderbilt University, and the Oak Ridge National Laboratory, and is supported by them and DOE.

[1] E.S. Paul, R. Ma, C.W. Beausang, D.B. Fossan, W.F. Piel, Jr., S. Shi, N. Xu, and J.-Y. Zhang, Phys. Rev. Lett. **61**, 42 (1988).

[2] R.A. Bark, G.D. Dracoulis, A.E. Stuchbery, A.P. Byrne, A.M. Baxter, F. Riess, and P.K. Weng, J. Phys. G **15**, L169 (1989); Nucl. Phys. **A501**, 157 (1989).

[3] L. Hildingsson, W. Klamra, Th. Lindblad, C.G. Lindén, C.A. Kalfas, S. Kossionides, C.T. Papadopoulos, R. Vlastou, J. Gizon, D. Clarke, F. Khazaie, and J.N. Mo, Nucl. Phys. **A513**, 394 (1990).

[4] H.-Q. Jin, L.L. Riedinger, C.-Y. Yu, W. Nazarewicz, R. Wyss, J.-Y. Zhang, C. Baktash, J.D. Garrett, N.R. Johnson, I.Y. Lee, and F.K. McGowan, Phys. Lett. B **277**, 387 (1992).

[5] S. Juutinen, P. Ahonen, J. Hattula, R. Julin, A. Pakkanen, A. Virtanen, J. Simpson, R. Chapman, D. Clarke, F. Khazaie, J. Lisle, and J.N. Mo, Nucl. Phys. **A526**, 346 (1991).

[6] B. Cederwall, B. Fant, R. Wyss, A. Johnson, J. Nyberg, J. Simpson, A.M. Bruce, and J.N. Mo, Phys. Rev. C **43**, R2031 (1991).

[7] G.D. Dracoulis, B. Fabricius, T. Kibedi, A.M. Baxter, A.P. Byrne, K.P. Lieb, and A.E. Stuchbery, Nucl. Phys. **A534**, 173 (1991).

[8] W. Waluś, L. Carlén, S. Jónsson, J. Lyttkens, H. Ryde, J. Kownacki, W. Nazarewicz, J.C. Bacelar, J. Dudek, J.D. Garrett, G.B. Hagemann, B. Herskind, and C.X. Yang, Phys. Scr. **34**, 710 (1986).

[9] R.A. Bark, G.B. Hagemann, H.J. Jensen, W. Korten, J. Wrzesinski, H. Carlsson, M. Bergström, A. Brockstedt, A. Nordlund, H. Ryde, P. Bosetti, S. Leoni, F. Ingebretsen, and P.O. Tjøm, Nucl. Phys. **A591**, 265 (1995).

[10] R. Kaczarowski, U. Garg, E.G. Funk, and J.W. Mihelich, Phys. Rev. C **45**, 103 (1992).

[11] G.D. Dracoulis, B. Fabricius, T. Kibédi, A.P. Byrne, and A.E. Stuchbery, Nucl. Phys. **A554**, 439 (1993).

[12] G.D. Dracoulis, B. Fabricius, A.P. Byrne, A.E. Stuchbery, A.M. Baxter, K.P. Lieb, K.J. Schiffer, and T. Kibedi, Phys. Lett. B **257**, 21 (1991).

[13] G.D. Dracoulis, R.A. Bark, A.E. Stuchbery, A.P. Byrne, A.M. Baxter, and F. Riess, Nucl. Phys. **A486**, 414 (1988).

[14] R. Bengtsson, Nucl. Phys. **A520**, 201c (1990); R. Wyss (private communication).

[15] V.P. Janzen, M.P. Carpenter, L.L. Riedinger, W. Schmitz, S. Pilotte, S. Monaro, D.D. Rajnauth, J.K. Johansson, D.G. Popescu, J.C. Waddington, Y.S. Chen, F. Dönau, and P.B. Semmes, Phys. Rev. Lett. **61**, 2073 (1988).

[16] A.J. Kreiner, J. Davidson, M. Davidson, P. Thieberger, and E.K. Warburton, Phys. Rev. C **42**, 878 (1990); A.J. Kreiner, Nucl. Phys. **A520**, 225c (1990).

[17] V.P. Janzen, Z.-M. Liu, M.P. Carpenter, L.H. Courtney, H.-Q. Jin, A.J. Larabee, L.L. Riedinger, J.K. Johansson, D.G. Popescu, J.C. Waddington, S. Monaro, S. Pilotte, and F. Dönau, Phys. Rev. C **45**, 613 (1992).

[18] G. Palameta and J.C. Waddington, Nucl. Instrum. Methods A **234**, 476 (1985).

[19] U. Bosch-Wicke, W.-D. Schmidt-Ott, F. Meissner, H. Salewski, and R. Michaelsen, Z. Phys. A **341**, 245 (1992).

[20] L.L. Riedinger, H.-Q. Jin, and C.-H. Yu, Nucl. Phys. **A520**, 287c (1990).

[21] D. Müller, A. Virtanen, R. Julin, S. Juutinen, M. Piiparinen, S. Törmänen, F. Christancho, A.P. Byrne, G.D. Dracoulis, B. Fabricius, C. Fahlander, A. Johnson, K.P. Lieb, J. Nyberg, I. Thorslund, and R. Wyss, Phys. Lett. B **332**, 265 (1994).

[22] W. Nazarewicz, M.A. Riley, and J.D. Garrett, Nucl. Phys. **A512**, 61 (1990).

[23] G.D. Dracoulis, C. Fahlander, and M.P. Fewell, Nucl. Phys. **A383**, 119 (1982).

[24] M.P. Carpenter *et al.*, ORNL Phys. Div. Prog. Report ORNL-6326, 1986, p. 82; L. Zhou *et al.*, University of Tennessee Prog. rep. 1988, p.21.

[25] A.C. Kahler, L.L. Riedinger, N.R. Johnson, R.L. Robinson, E.F. Zganjar, A. Visvanathan, D.R. Zolnowski, M.B. Hughes, and T.T. Sugihara, Phys. Lett. **72B**, 443 (1978).

[26] A.J. Larabee, M.P. Carpenter, L.L. Riedinger, L.H. Courtney, J.C. Waddington, V.P. Janzen, W. Nazarewicz, J.-Y. Zhang, R. Bengtsson, and G.A. Leander, Phys. Lett. **169B**, 21 (1986).

[27] J.K. Johansson, D.G. Popescu, D.D. Rajnauth, J.C. Waddington, M.P. Carpenter, L.H. Courtney, V.P. Janzen, A.J. Larabee, Z.M. Liu, and L.L. Riedinger, Phys. Rev. C **40**, 132 (1989).

[28] T. Bengtsson and I. Ragnarsson, Nucl. Phys. **A436**, 14 (1985).

[29] J.-Y. Zhang, A.J. Larabee, and L.L. Riedinger, J. Phys. G **13**, L75 (1987).

[30] J.L. Wood, E.F. Zganjar, and J.D. Cole, Bull. Am. Phys. Soc. **25**, 739 (1980).

[31] G.D. Dracoulis and B. Fabricius, Phys. Rev. C **41**, 2933 (1990).

[32] H.J. Jensen, G.B. Hagemann, P.O. Tjøm, S. Frauendorf, A. Atac, M. Bergström, A. Bracco, A. Brockstedt, H. Carlsson, P.

Ekström, J.M. Espino, B. Herskind, F. Ingebretsen, J. Jongman, S. Leoni, R.M. Lieder, T. Lönnroth, A. Maj, B. Million, A. Nordlund, J. Nyberg, M. Piiparinen, H. Ryde, M. Sugawara, and A. Virtanen, Z. Phys. A **340**, 351 (1991).

[33] J. Gascon, C.-H. Yu, G.B. Hagemann, M.C. Carpenter, J.M. Espino, Y. Iwata, T. Komatsubara, J. Nyberg, S. Ogaza, G. Sletten, P.O. Tjøm, D.C. Radford, J. Simpson, A. Alderson, M.A. Bentley, P. Fallon, P.D. Forsyth, J.W. Roberts, and J.F. Sharpey-Schafer, Nucl. Phys. **A513**, 344 (1990).

[34] R. Bengtsson and S. Frauendorf, Nucl. Phys. **A314**, 27 (1979); **A327**, 139 (1979).

[35] P.H. Regan, R. Wadsworth, S.M. Mullins, J. Nyberg, A. Atac, S.A. Forbes, D.B. Fossan, Y.-J. He, J.R. Hughes, I. Jenkins, R. Ma, M.S. Metcalfe, P.J. Nolan, E.S. Paul, R.J. Poynter, D. Santonicio, A. Virtanen, and N. Xu, J. Phys. G **18**, 847 (1992).

[36] C.-H. Yu, G.B. Hagemann, J.M. Espino, K. Furuno, J.D. Garrett, R. Chapman, D. Clarke, F. Khazaie, J.C. Lisle, J.N. Mo, M. Bergström, L. Carlén, P. Ekström, J. Lyttkens, and H. Ryde, Nucl. Phys. **A511**, 157 (1990).

[37] J.C. Bacelar, R. Chapman, J.R. Leslie, J.C. Lisle, J.N. Mo, E. Paul, A. Simcock, J.C. Willmott, J.D. Garrett, G.B. Hagemann, B. Herskind, A. Holm, and P.M. Walker, Nucl. Phys. **A442**, 547 (1985).

[38] Y. Sun, S. Wen, and D.H. Feng, Phys. Rev. Lett. **72**, 3483 (1994).

[39] P.H. Stelson and L. Grodzins, Nucl. Data **A1**, 21 (1965).

[40] R. Kaczarowski, U. Garg, A. Chaudhury, E.G. Funk, J.W. Mihelich, D. Frekers, R.V.F. Janssens, and T.L. Khoo, Phys. Rev. C **41**, 2069 (1990).

[41] R. Wyss, W. Satula, W. Nazarewicz, and A. Johnson, Nucl. Phys. **A511**, 324 (1990).

[42] G.D. Dracoulis, A.E. Stuchbery, A.P. Byrne, A.R. Poletti, S.J. Poletti, J. Gerl, and R.A. Bark, J. Phys. G **12**, L97 (1986).

[43] R. Bengtsson, J.-Y. Zhang, J.H. Hamilton, and L.K. Peker, J. Phys. G **12**, L223 (1986).

[44] R.A. Bark, R. Bengtsson, and H. Carlsson, Phys. Lett. B **339**, 11 (1994).

[45] M.P. Carpenter, C.R. Bingham, L.H. Courtney, V.P. Janzen, A.J. Larabee, Z.-M. Liu, L.L. Riedinger, W. Schmitz, R. Bengtsson, T. Bengtsson, W. Nazarewicz, J.-Y. Zhang, J.K. Johansson, D.G. Popescu, J.C. Waddington, C. Baktash, M.L. Halbert, N.R. Johnson, I.Y. Lee, Y.S. Schutz, J. Nyberg, A. Johnson, J. DeBuc, S. Monaro, S. Pilotte, K. Honkanen, D.G. Sarantites, and D.R. Haenni, Nucl. Phys. **A513**, 125 (1990).

[46] S.E. Larsson, G. Leander, and I. Ragnarsson, Nucl. Phys. **A307**, 189 (1978).

[47] I. Ragnarsson and P.B. Semmes, Hyperfine Interact. **43**, 425 (1988).

[48] F. Dönau and S. Frauendorf, Phys. Lett. **71B**, 263 (1977).

[49] P.B. Semmes, Lecture Notes at Hands on Nucl. Struc. Theory Workshop, Oak Ridge, Aug. 5–16, 1991 (unpublished).

[50] U. Garg, W. Reviol, and P.B. Semmes, Phys. Rev. C **47**, 2407 (1993).